7-26-2019

Super-Enhancer-Associated LncRNA UCA1 Interacts Directly with AMOT to Activate YAP Target Genes in Epithelial Ovarian Cancer.

Xianzhi Lin

Tassja J. Spindler

Marcos A. de Souza Fonseca

Rosario I. Corona

Ji-Heui Seo

See next page for additional authors

Recommended Citation

Authors

Xianzhi Lin, Tassja J. Spindler, Marcos A. de Souza Fonseca, Rosario I. Corona, Ji-Heui Seo, Felipe S. Dezem, Lewyn Li, Janet M. Lee, Henry W. Long, Thomas A. Sellers, Beth Y. Karlan, Houtan Noushmehr, Matthew L. Freedman, Simon A. Gayther, and Kate Lawrenson

iScience

Article

Super-Enhancer-Associated LncRNA *UCA1* Interacts Directly with AMOT to Activate YAP Target Genes in Epithelial Ovarian Cancer

Xianzhi Lin,[1] Tassja J. Spindler,[1] Marcos Abraão de Souza Fonseca,[2] Rosario I. Corona,[1,3] Ji-Heui Seo,[4] Felipe Segato Dezem,[2] Lewyn Li,[4] Janet M. Lee,[3] Henry W. Long,[4,5] Thomas A. Sellers,[6] Beth Y. Karlan,[1] Houtan Noushmehr,[2,7] Matthew L. Freedman,[4,5,8] Simon A. Gayther,[3] and Kate Lawrenson[1,3,9,*]

SUMMARY

Long noncoding RNAs (lncRNAs) have emerged as critical regulators of tumorigenesis, and yet their mechanistic roles remain challenging to characterize. Here, we integrate functional proteomics with lncRNA-interactome profiling to characterize *Urothelial Cancer Associated 1* (*UCA1*), a candidate driver of ovarian cancer development. Reverse phase protein array (RPPA) analysis indicates that *UCA1* activates transcription coactivator YAP and its target genes. *In vivo* RNA antisense purification (iRAP) of *UCA1* interacting proteins identified angiomotin (AMOT), a known YAP regulator, as a direct binding partner. Loss-of-function experiments show that AMOT mediates YAP activation by *UCA1*, as *UCA1* enhances the AMOT-YAP interaction to promote YAP dephosphorylation and nuclear translocation. Together, we characterize *UCA1* as a lncRNA regulator of Hippo-YAP signaling and highlight the *UCA1*-AMOT-YAP signaling axis in ovarian cancer development.

INTRODUCTION

Long noncoding RNAs (lncRNAs) are a class of noncoding transcripts over 200 nucleotides in length. They are expressed in a highly tissue- and disease-specific manner and play critical roles in development and disease (Derrien et al., 2012, 2012; Guttman et al., 2010, 2009; Kretz et al., 2012; Loewer et al., 2010). In cancer, dysregulated lncRNAs can function either as oncogenes (Calin et al., 2007; Gupta et al., 2010; Wang et al., 2008) or tumor suppressors (Kotake et al., 2011; Wang et al., 2012). LncRNAs have emerged as critical regulators of gene expression, with their activity largely governed by absolute expression levels, interacting partners, and subcellular localization (Guttman and Rinn, 2012).

Epithelial ovarian cancer (EOC) is the most lethal gynecological malignancy in the United States, with less than 50% of patients surviving more than 5 years (Siegel et al., 2016). This is largely due to lack of effective targeted therapies for treatment of EOC, which is often drug resistant when it recurs. So far, a handful of lncRNAs have been implicated in EOC. *H19* and *HOTAIR* are expressed in ovarian tumors (Qiu et al., 2014; Tanos et al., 1999), and *MEG3*, *DNM3OS*, and *MIAT* are critical for epithelial-to-mesenchymal transition (Mitra et al., 2017). However, the underlying functional mechanisms of lncRNAs in EOC development remains poorly understood and their prospects as therapeutic targets for ovarian cancer unexplored.

For each tumor type there are typically thousands of dysregulated lncRNAs, but there is currently no consensus on the most efficient approach to identifying and characterizing the most critical players in disease development. Here, we implement a strategy for prioritization and characterization of lncRNAs implicated in cancer. The "LncRNA Interpreter" approach combines functional proteomics with interactome profiling to characterize the functional and biological role of a candidate lncRNA. We established and validated this strategy using lncRNA *Urothelial Cancer Associated 1* (*UCA1*) as a proof of concept. We found *UCA1* overexpression is a driver of ovarian cancer development. The reverse phase protein array (RPPA) profiling revealed deregulation of Hippo-YAP signaling when *UCA1* is depleted. Characterization of *UCA1* interacting proteins identified a mechanism of regulation of Hippo-YAP signaling *via* physical interactions between *UCA1* and angiomotin (AMOT), a non-canonical RNA-binding protein. The LncRNA Interpreter approach can therefore efficiently provide critical mechanistic insights for characterization of candidate lncRNAs.

[1]Women's Cancer Program at the Samuel Oschin Comprehensive Cancer Institute, Cedars-Sinai Medical Center, Los Angeles, CA, USA

[2]Department of Genetics, University of Sao Paulo, Ribeirao Preto, Sao Paulo, Brazil

[3]Center for Bioinformatics and Functional Genomics, Samuel Oschin Comprehensive Cancer Institute, Cedars-Sinai Medical Center, Los Angeles, CA, USA

[4]Department of Medical Oncology, Dana-Farber Cancer Institute and Harvard Medical School, Boston, MA, USA

[5]Center for Functional Cancer Epigenetics, Dana-Farber Cancer Institute, Boston, MA, USA

[6]Department of Cancer Epidemiology, Moffitt Cancer Center, Tampa, FL, USA

[7]Department of Neurosurgery, Henry Ford Health System, Detroit, MI, USA

[8]The Eli and Edythe L. Broad Institute, Cambridge, MA, USA

[9]Lead Contact

*Correspondence: kate.lawrenson@cshs.org

https://doi.org/10.1016/j.isci.2019.06.025

RESULTS

LncRNA Interpreter, a Strategy for Mechanistic Analysis of LncRNAs

An overview of LncRNA Interpreter strategy is shown in Figure 1. Following lncRNA identification (e.g., from analysis of patient data or analyses of super-enhancer-associated lncRNAs), lncRNA knockout (KO) models are generated for disease-relevant phenotypic characterization. The RPPA is utilized to evaluate differentially expressed proteins and downstream pathways affected by disruption of lncRNAs. Most key cancer pathways are surveyed on the RPPA (Paweletz et al., 2001), which enables quantification of several protein post-translational modifications that are crucial for signaling cascades commonly deregulated in cancer (Charboneau et al., 2002). We developed *in vivo* RNA antisense purification (iRAP) from previously developed RNA-centric methods (Chu et al., 2015; McHugh et al., 2015; Minajigi et al., 2015) to catalog the interacting proteome of candidate lncRNAs. As protein-RNA interactions are essential for lncRNA functionality, intersection of proteins/pathways identified using RPPA with iRAP profiles provides an efficient approach for dissecting the underlying mechanism of candidate lncRNAs implicated in complex diseases such as cancer.

UCA1 Is a Driver of Ovarian Cancer Development and Outcome

We evaluated data from The Cancer Genome Atlas (Cancer Genome Atlas Research Network, 2011) to identify candidate lncRNAs that drive the development and clinical outcome (survival) in high-grade serous EOC cases. We identified an lncRNA signature comprising 50 lncRNAs associated with patient prognosis (Figure 2A, Table S1). Since super-enhancers mark pivotal oncogenes in many tumor types (Jiang et al., 2018; Lovén et al., 2013; Peng et al., 2019; Xie et al., 2018), we integrated lncRNA expression data with genome-wide profiles of enhancer marks generated using chromatin immunoprecipitation sequencing (ChIP-seq) for H3K27ac in primary high-grade serous EOC tissues to identify super-enhancers that drive candidate oncogenic lncRNA expression. Ninety-three super-enhancers identified in high-grade serous EOC tissues were associated with lncRNA expression (Figure 2A, Table S2), of which three, *UCA1*, *SNHG9*, and *SNHG15*, were also associated with prognosis (Figure 2A, Table S1). *UCA1* is of particular interest as this lncRNA has been implicated in the development of other cancers (Chen et al., 2016; Fang et al., 2014; Han et al., 2014; Hughes et al., 2015; Li et al., 2014, 2016a, 2016b; Na et al., 2015; Nie et al., 2016; Tian et al., 2014; Tuo et al., 2015; Wang et al., 2015; Zhang et al., 2016; Zhao et al., 2017; Zheng et al., 2015), although its functional targets remain elusive. The *UCA1* locus is marked by a super-enhancer in all major histotypes of ovarian cancer—clear cell, endometrioid, high-grade serous, and mucinous—but not in precursor tissues—fallopian tube secretory epithelial cells (FTSECs) or ovarian surface epithelial cells (OSECs) (Figure 2B). *UCA1* expression positively correlates with super-enhancer signal at this locus ($r = 0.51$, $p = 0.026$, Spearman's correlation) (Figure 2C), suggesting that this tumor-specific super-enhancer regulates *UCA1* expression. Super-enhancer-associated genes are particularly responsive to treatment of (+)-JQ1 (Lovén et al., 2013), a potent inhibitor of BET family of bromodomain proteins including BRD4 (Filippakopoulos et al., 2010); we found that *UCA1* expression was significantly downregulated in two ovarian cancer cell lines treated with (+)-JQ1 compared with dimethyl sulfoxide (DMSO)-treated control cells (Figure 2D). The expression of a neighboring gene *OR10H1* (∼20 kb upstream), which has no super-enhancer at its locus (Figure S1A) and shows some evidence of correlation with the *UCA1* super-enhancer ($r = 0.47$, $p = 0.043$, Spearman's correlation) (Figure S1B), was not affected by (+)-JQ1 treatment (Figure 2D). Together these analyses suggesting the super-enhancer at this locus drives the expression of *UCA1* in ovarian cancer.

Deletion of *UCA1* Impairs Ovarian Cancer Cell Growth

CRISPR/Cas9 genome editing was used to create stable *UCA1* KO models in ovarian cancer cell lines OVCA429 and OVISE (Figures 3A and 3B). *UCA1* expression was undetectable in all *UCA1* KO models (Figure 3C). The effects of *UCA1* KO on *in vivo* tumor cell growth were established after intra-peritoneal injection of 10 million wild-type (WT) *UCA1* or *UCA1* KO cells in nude mice. The mass of resulting tumors was significantly smaller in *UCA1* KO models compared with those in mice injected with WT cells (OVCA429 $p = 0.002$; OVISE $p = 0.002$) (Figures 3D and 3E), indicating that *UCA1* acts as a potent promoter of tumor seeding and/or growth *in vivo*.

UCA1 Regulates Hippo-YAP Signaling in Ovarian Cancer

We used RPPAs to profile changes in protein abundance and phosphorylation following *UCA1* KO. The most differentially expressed proteins between WT and *UCA1* KO cells included phosphorylated YAP at

A Discovery of Dysregulated LncRNAs

Clinical data (*RNA-Seq, Survival*)

Disease tissue/cell **vs** Normal tissue/cell (*H3K27ac ChIP-Seq & RNA-Seq*)

Prognostic lncRNAs

Super-enhancer-associated lncRNAs

Candidate lncRNAs

B Phenotypic Characterization

LncRNA KO

Cas9 gRNA 3'

Target lncRNA 5' 5' DNA

3' 5' 3'

NGG PAM

Cleavage

Phenotypic characterization *in vitro & in vivo*

C RPPA

WT cell lysate **vs** KO cell lysate

Validated antibodies

Quantification

Candidate target proteins

D iRAP

UV crosslinking

RBP RBP RBP

Homogenization by sonication

Biotinylated antisense probes

Hybridization RBP RBP RBP 37°C 4h

Streptavidin Dynabeads

Capture RBP RBP RBP 37°C 30 min

Elution RBP RBP RBP

Analysis Proteins RNA

MS or WB RT-qPCR

Candidate lncRNA-associated proteins

E Common Protein Targets and/or Pathways

Validation by WB and RIP

Functional verification by loss of function and gain of function experiments
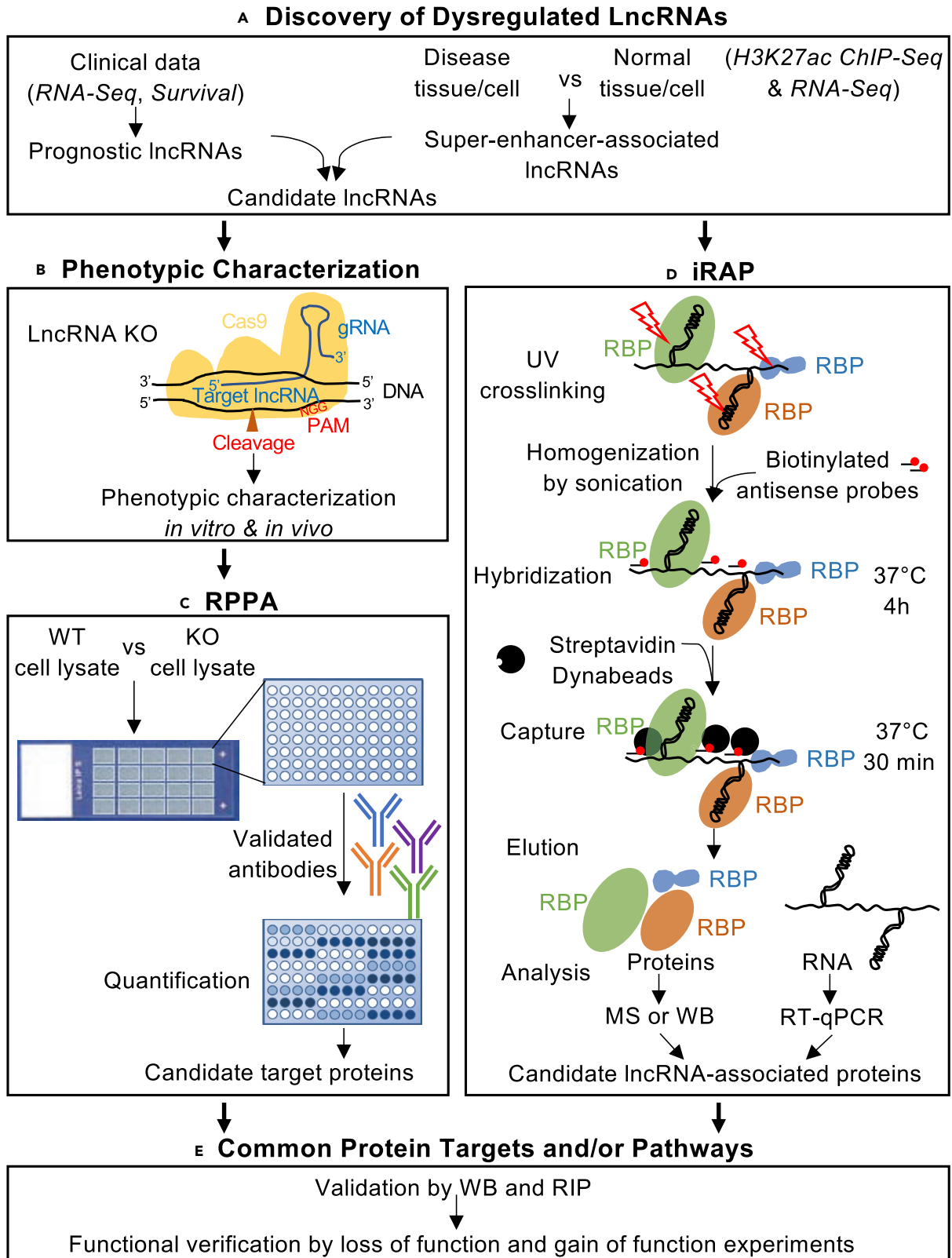
Figure 1. LncRNA Interpreter, a Strategy for Mechanistic Analysis of lncRNAs

The LncRNA Interpreter strategy consists of five major components. (A) Discovery of candidate lncRNAs is performed using patient specimens. (B) Phenotypic characterization of the candidate lncRNA is performed *in vitro* and *in vivo* using KO cancer cell models generated using CRISPR/Cas9 genome editing technique. (C) Proteins affected by candidate lncRNA are identified by functional proteomics using RPPA. (D) LncRNA interacting proteins are identified using iRAP. (E) RPPA and iRAP data are integrated to identify common protein targets. ChIP-seq, chromatin immunoprecipitation sequencing; RNA-Seq, RNA sequencing; RPPA, reverse phase protein array; iRAP, *in vivo* RNA antisense purification; WT, wild-type; KO, knockout; RBP, RNA-binding protein; RIP, RNA immunoprecipitation; MS, mass spectrometry; WB, western blotting; RT-qPCR, reverse transcription quantitative polymerase chain reaction.

Ser127 (YAPpS127, fold change [FC] = 1.3, p = 0.038), AXL (FC = 0.75, p = 0.031), and PUMA (FC = 1.18, p = 0.042), all of which belong to the Hippo-YAP signaling pathway (Figure 4A, Table S3). YAPpS127 is retained in the cytoplasm via binding to 14-3-3 protein, which leads to inhibition of downstream YAP signaling (Zhao et al., 2010). We observed an increased expression of YAPpS127 and pro-apoptotic YAP target gene PUMA (Matallanas et al., 2007) and decreased expression of the pro-proliferative YAP target gene AXL (Xu et al., 2011) in *UCA1* KO compared with WT cells (Figure 4A), indicating that *UCA1* activates Hippo-YAP signaling for cell survival and proliferation. Consistent with this, YAPpS127 protein expression is significantly lower in primary tumors with *UCA1* overexpression or amplification (n = 105, average abundance −0.25) compared with tumors with no *UCA1* overexpression (n = 477, average abundance 0.07, p = 2.8×10^{-4}, Q = 0.019) (Figure S2A). There was no significant difference in total YAP protein expression between the two groups (Figure S2B), suggesting that *UCA1* also activates YAP signaling *in vivo*.

Since the presence of a non-unique intronic sequence mandated the introduction of a >5 kb deletion to KO *UCA1*, it is plausible that noncoding elements within the *UCA1* locus activate YAP target genes in *cis* or in *trans*. To test this possibility, loss-of-function experiments using small interfering RNAs (siRNAs) specific to *UCA1* were conducted to validate the role of *UCA1* in regulation of Hippo-YAP signaling. After *UCA1* knockdown (KD) in high-grade serous ovarian cancer cell lines (Figure 4B), total YAP expression was unaltered, whereas YAPpS127 was elevated at least 50% in all three ovarian cancer cell lines (by ImageJ) (Figure 4C), consistent with RPPA results in *UCA1* KO cells and primary tissues. YAP regulates the expression of AXL and CYR61 at both RNA (Figure 4D) and protein levels (Figure 4E), indicating that AXL and CYR61 are indeed YAP targets in ovarian cancer. The effect of *UCA1* KD on the abundance of AXL and CYR61 largely phenocopied YAP KD (Figures 4C and 4E). Moreover, gain-of-function experiments performed by overexpressing *UCA1* in TERT-immortalized, MYC-expressing normal ovarian epithelial cells (OSEC4C2) (Figure 4F) demonstrated that overexpression of *UCA1* increased the expression of YAP target genes AXL, CYR61, as well as CTGF (Figure 4G). Consistent with the loss-of-function experiments, overexpression of *UCA1* inhibits YAP phosphorylation but does not affect total YAP expression (Figure 4G). Taken together, these data indicate that *UCA1* activates Hippo-YAP signaling in ovarian cancer.

iRAP Catalogs the *UCA1* Interacting Proteome

Proteins purified from two independent *UCA1*-iRAP experiments were profiled by mass spectrometry. Each iRAP experiment included two non-overlapping *UCA1* probe sets (*UCA1*-odd, *UCA1*-even) for cross-validation and a *U1* probe as positive control (Figure S3A, Table S4). The iRAP assay was highly specific: both *UCA1* probe sets significantly enriched *UCA1* but not *U1* snRNA; conversely, the *U1* probe enriched *U1* snRNA but not *UCA1*. As expected, *U6* snRNA was not enriched by any of the probes (Figure S3B). iRAP-MS recovered 86 *U1*-associated proteins (Figure 5A), including six known *U1* direct binding proteins and another 35 *U1*-associated proteins (Figure S3C, Table S5) (Chu et al., 2015). These data indicate that iRAP efficiently identifies *bona fide* RNA-binding proteins associated with a specific target transcript. We isolated 47 and 42 proteins, respectively, using *UCA1*-odd and *UCA1*-even probe sets (Figure 5A). Thirty-eight proteins were only associated with *UCA1*, 19 of which were identified by both sets of probes (Figure 5A). In most instances the same peptide was retrieved by both *UCA1* probe sets across the two experiments (Figures 5B and S3D, Table S5), suggesting that these 19 proteins are true *UCA1*-binding proteins.

UCA1 Interacts Directly with Hippo-YAP Signaling Regulator AMOTp130

We intersected the *UCA1* interacting proteome with the pathways identified in the RPPA profiling described earlier. This highlighted AMOT, a known regulator of Hippo-YAP signaling (Moleirinho et al., 2017; Zhao et al., 2011). A peptide mapping to amino acids 727–740 of AMOT was identified by both *UCA1* probe sets in two independent experiments (Figure 5B), suggesting this predicted coiled-coil
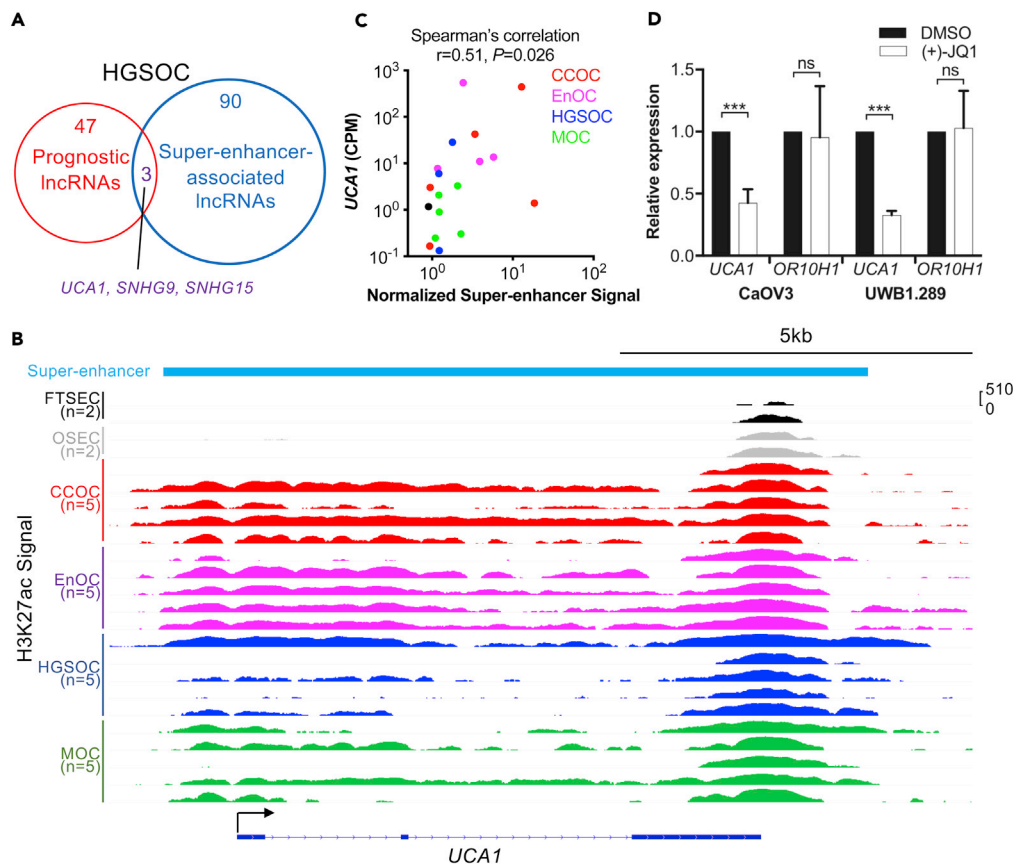
Figure 2. *UCA1* in Ovarian Cancer Development and Outcome

(A) In high-grade serous EOCs a signature of 50 lncRNAs was prognostic. Using tumor tissue H3K27ac data, 93 high-grade serous EOC super-enhancer-associated lncRNAs were identified. 3 lncRNAs were shared between the two analyses.

(B) *UCA1*-associated super-enhancer is present across the four major histological subtypes of EOC, but not normal precursor cells. H3K27ac ChIP-seq signal is shown in log scale. CCOC, clear cell ovarian cancer; EnOC, endometrioid ovarian cancer; HGSOC, high-grade serous ovarian cancer; MOC, mucinous ovarian cancer.

(C) Super-enhancer signal positively correlates with *UCA1* expression (Spearman's correlation, r = 0.51, p = 0.026). Counts per million (CPM) of *UCA1* from RNA-seq is shown. Super-enhancer signals were normalized using TMM (Robinson and Oshlack, 2010). We did not have sufficient tissue to do RNA-seq for one EnOC tumor (#3), and one HGSOC tumor (#4) does not express *UCA1*.

(D) *UCA1* expression is sensitive to JQ1 treatment in HGSOC models. Two HGSOC cell lines (CaOV3, UWB1.289) were treated with (+)-JQ1 or DMSO. The expression of *UCA1* and *OR10H1* was measured by RT-qPCR.

Data shown here are mean $\pm$ SD from three independent experiments. ***p = 1×10^{-7} (CaOV3), ***p = 2×10^{-8} (UWB1.289), ns, not significant, Student's t test. See also Figure S1, Tables S1 and S2.

domain of AMOT is responsible for the interaction with *UCA1*. AMOT exists as two isoforms, AMOTp130 and AMOTp80, a shorter isoform that lacks 409 amino acids at the N terminus due to alternative splicing of the *AMOT* gene between exon 2 and 3 (Ernkvist et al., 2006). Western blotting of iRAP lysates validated the AMOT-*UCA1* interaction. We observed shifted AMOTp130 (to around 160 kDa) but not AMOTp80, suggesting that *UCA1* associates specifically with AMOTp130 (Figure 5C). To further verify the AMOT-*UCA1* interaction, we performed RNA immunoprecipitation (RIP) using an anti-AMOT antibody (Table S6). Western blotting for AMOT confirmed successful pull-down of both AMOTp80 and AMOTp130 isoforms (Figure 5D), and an ~2- to 5-fold enrichment of *UCA1* was detected in AMOT-RIP samples compared with corresponding control isotype IgG pulldowns (CaOV3, p = 7.4×10^{-6}; OVCA429, p = 0.011; UWB1.289, p = 7.2×10^{-7}) (Figure 5E). We noted that a higher ratio of AMOTp130/p80 correlates with a higher fold enrichment of *UCA1* (Figures 5D and 5E), further suggesting that *UCA1* preferentially associates with AMOTp130. To validate this, we overexpressed GFP-AMOTp130 or GFP-AMOTp80 in
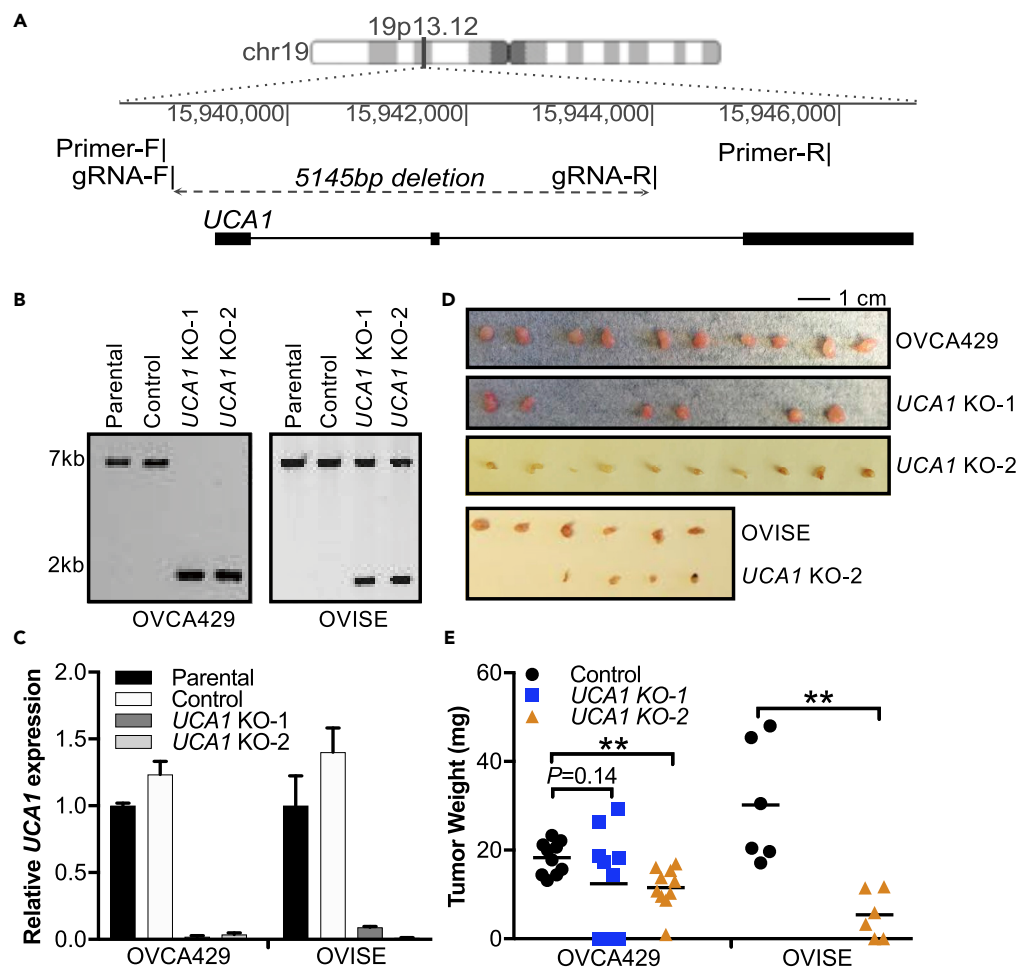
Figure 3. Inactivation of *UCA1* Impairs Ovarian Cancer Cell Growth

(A) Schematic of CRISPR/Cas9 genome editing strategy for *UCA1* knockout.

(B) Long-range PCR of parental (OVCA429 and OVISE) cells, control cells expressing the gRNA vector backbone, and two stable *UCA1* knockout clones from each cell line (*UCA1* KO-1, *UCA1* KO-2).

(C) The expression of *UCA1*, measured by RT-qPCR, was normalized to the expression of GAPDH and β-actin in the *UCA1* KO models, parental cells, and control cells. Data shown are mean ± SD from three independent experiments.

(D) Images of excised tumors from mouse xenograft model. Scale bar represents 1 cm.

(E) Tumor weight of xenografted *UCA1* KO ovarian cancer cells and parental controls. **p < 0.01, Student's t test.

EOC cells and performed GFP-RIP. Western blotting validated successful pull-down of both GFP-AMOTp80 and GFP-AMOTp130 (Figure 5F) with significant enrichment of *UCA1* observed for GFP-AMOTp130 but not GFP-AMOTp80 (Figure 5G), despite the markedly more efficient pull-down of AMOTp80 (Figure 5F). These data together indicate that *UCA1* interacts directly with AMOTp130 but not AMOTp80.

AMOTp130 but not AMOTp80 was previously reported to interact with YAP and regulate its activity (Sowa et al., 2009; Zhao et al., 2011). We tested whether this interaction is intact in EOC. In YAP-RIP experiments, AMOTp130 was detected in YAP pull-downs (Figure 5H), confirming that YAP interacts with AMOTp130. AMOTp80 was also detected in YAP pull-downs for two of the three cell lines, which may be due to hetero-oligomerization (Ernkvist et al., 2008; Patrie, 2005; Zheng et al., 2009). Interestingly, a 4- to 29-fold enrichment of *UCA1* was detected in YAP pulldowns compared with IgG isotype controls (Figure 5I). Since we did not identify YAP using iRAP (which preferentially detects direct binding proteins), these data suggest that YAP, AMOTp130, and *UCA1* form a trimer complex with AMOTp130 bridging the interaction between YAP and *UCA1*. Once formed, the AMOTp130-YAP interaction is independent of *UCA1* since the association still exists following RNase A treatment (Figures 5J and 5K).
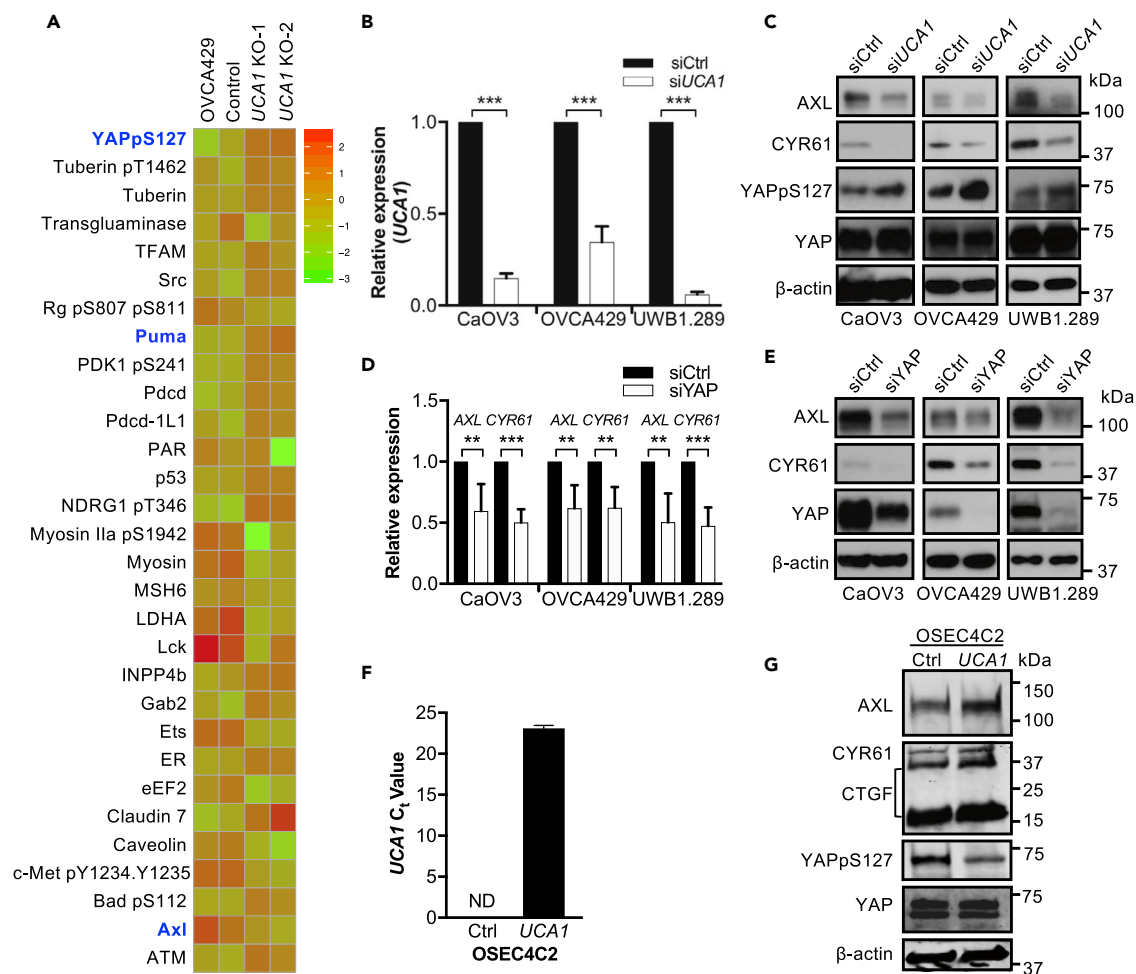
Figure 4. UCA1 Activates Hippo-YAP Signaling in Ovarian Cancer

(A) RPPA analyses of OVCA429 UCA1 KO cells and controls. All proteins with significant changes (FC > 1.2 or <0.9 and p ≤ 0.05) in abundance are shown. Proteins highlighted in blue are involved in Hippo-YAP signaling.

(B) The expression of UCA1 was measured by RT-qPCR and normalized to β-actin in both scramble control siRNA (siCtrl) and UCA1-specific siRNA (siUCA1)-transfected CaOV3, OVCA429, and UBW1.289 cells. Data shown are mean ± SD from three independent experiments.

(C) The expression of YAP, YAPpSer127, and YAP targets by western blotting in both siCtrl and siUCA1-transfected cells. Representative results from three independent experiments are shown. When UCA1 was knocked down, YAPpSer127 expression was elevated 90% (p < 0.01), 150% (p < 0.001), and 50% (p < 0.05) in CaOV3, OVCA429, and UWB1.289 cells, respectively. Student's t test.

(D) The expression of YAP targets AXL and CYR61 was measured by RT-qPCR in siCtrl and siYAP-transfected cells and normalized to β-actin. Data shown are mean ± SD from three independent experiments. **p < 0.01, ***p < 0.001, Student's t test.

(E) The expression of YAP and YAP targets by western blotting in CaOV3, OVCA429, and UBW1.289 cells transfected with siCtrl or siYAP.

(F) The C_t values of UCA1 lncRNA in both OSEC4C2 control cells and OSEC4C2 cells with UCA1 overexpression. ND, not detected. Data shown are mean ± SD from three independent experiments and normalized to 18S rRNA.

(G) The expression of YAP, YAPpSer127, and YAP targets by western blotting in both OSEC4C2 control cells and OSEC4C2 cells with UCA1 overexpression. β-Actin was used as loading control for western blotting.

See also Figure S2 and Table S3.

UCA1 Activates YAP and Target Genes by Enhancing the AMOTp130-YAP Interaction to Promote YAP Dephosphorylation and Nuclear Translocation

We next tested whether AMOT is required for activation of YAP target genes by UCA1. Western blotting and RT-qPCR validated the successful depletion of AMOT (Figure 6A) and UCA1 (Figure 6B), respectively. Both UCA1 and AMOT KD resulted in reduced expression of AXL and CYR61 and elevated the expression of YAPpS127 40%–100% but had no effect on total expression levels of YAP, YAP kinase LATS1, or active pLATS1 (Figure 6A). Although the expression of UCA1 was not affected by AMOT KD (Figure 6B), the
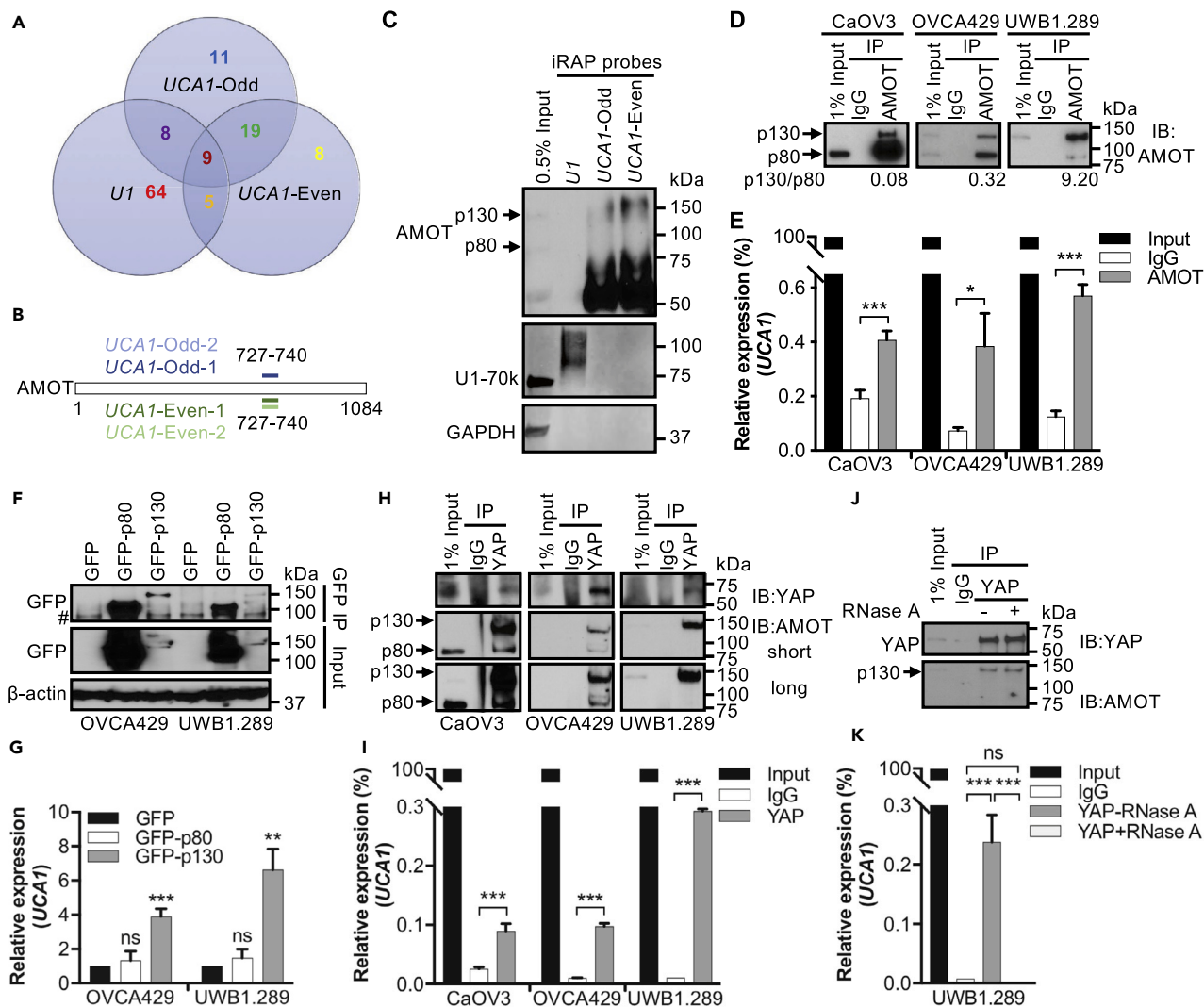
Figure 5. *UCA1* Interacts Directly with Hippo-YAP Signaling Regulator AMOTp130

(A) iRAP followed by mass spectrometry to catalog the *UCA1* interactome.

(B) The same AMOT peptides were reproducibly retrieved from *UCA1* iRAP. Numbers indicate the amino acid position; protein not drawn to scale. Data shown are from two independent experiments.

(C) Western blotting validation of AMOT as a direct binding protein for *UCA1* using iRAP samples. U1-70k, a known direct binding protein for *U1* snRNA, is used as positive control for *U1*. As expected, GAPDH binds neither *U1* nor *UCA1*.

(D and E) RIP validation of the AMOT-lncRNA *UCA1* interaction. (D) Western blotting validation of AMOT pull-down, using an AMOT specific antibody, in three high-grade serous EOC cell lines. Isotype IgG was included as negative control. Numbers beneath the blots are the relative ratios for AMOTp130:AMOTp80. (E) Relative expression of *UCA1* in AMOT immunoprecipitated RNA samples by RT-qPCR.

(F and G) RIP validation of AMOTp130-*UCA1* interaction. (F) Western blotting validation of GFP-tagged AMOT pull-down with an anti-GFP antibody. Representative images from three independent experiments are shown. Control cells were transduced with a GFP expressing vector only. (G) Relative expression of *UCA1* for GFP-RIP samples by RT-qPCR. # denotes a non-specific band observed with this GFP antibody. (H-I) RIP validation of YAP-AMOTp130-*UCA1* complex.

(H) Western blotting validation of YAP pull-down and AMOT co-immunoprecipitated using a YAP specific antibody. Isotype IgG was included as negative control.

(I) RT-qPCR measurement of relative expression of *UCA1* in YAP-RIP samples.

(J) RIP following RNase A treatment, *UCA1* is not required for the YAP-AMOTp130 interaction. Western blotting validation of YAP pull-down and AMOT co-immunoprecipitated by YAP specific antibody, with or without RNase A treatment. Isotype IgG was included as negative control.

(K) Relative expression of *UCA1* by RT-qPCR in YAP RIP samples, incubated with or without RNase A.

Data shown are mean ± SD from three independent experiments. *p < 0.05, **p < 0.01, ***p < 0.001, Student's t test. See also Figure S3, Tables S4 and S5.
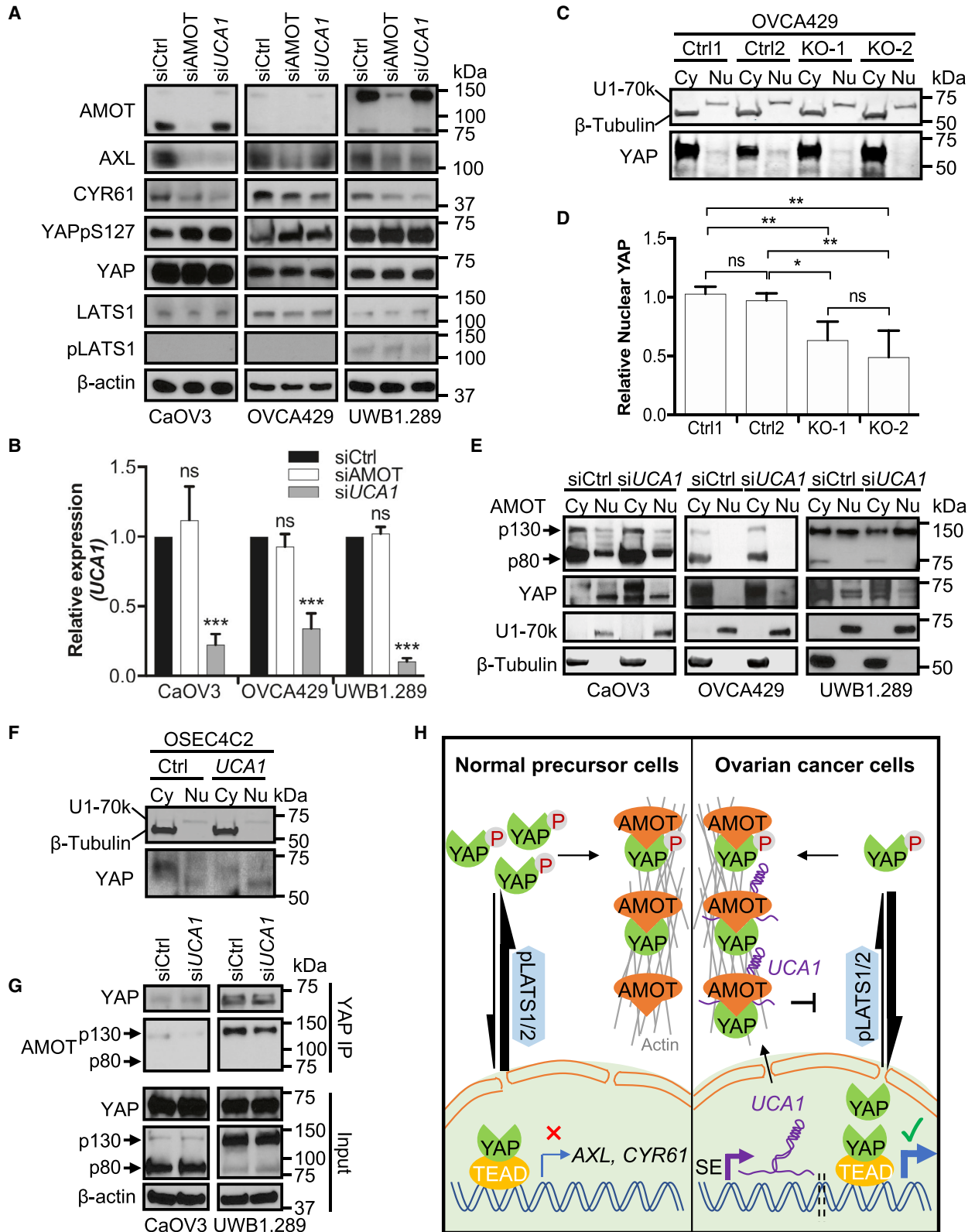
Figure 6. *UCA1* Activates YAP and Its Target Genes by Facilitating AMOTp130-YAP Interaction to Promote YAP Dephosphorylation and Nuclear Translocation

(A) AMOT mediates the activation of YAP and its target genes by *UCA1*. OC cells were transfected with siCtrl, siAMOT, or si*UCA1* for 72 h. Whole-cell lysates were prepared and blotted with antibodies indicated. When *UCA1* or AMOT is knocked down, YAPpSer127 expression is elevated 80% (p < 0.01), 100% (p < 0.01), and 40% (p < 0.01) in CaOV3, OVCA429, and UWB1.289 cells, respectively.

(B) Validation of siRNA knockdown efficiency for *UCA1*. Relative expression of *UCA1* by RT-qPCR for samples is shown in (A).

(C) *UCA1* KO in OVCA429 cells decreases nuclear YAP. *UCA1* wild-type (Ctrl1, Ctrl2) or knockout (KO-1, KO-2) OVCA429 cells were fractionated into cytoplasmic (Cy) and nuclear (Nu) fractions and blotted for β-tubulin (a cytoplasmic marker), U1-70k (a nuclear marker), and YAP.

(D) Quantification of nuclear YAP using ImageJ.

(E) *UCA1* KD decreases nuclear YAP. CaOV3, OVCA429, and UWB1.289 cells transfected with control siRNAs or si*UCA1* were fractionated into cytoplasmic and nuclear fractions and blotted for β-tubulin, U1-70k, AMOT, and YAP. Nuclear YAP is reduced 50% (CaOV3, p < 0.05) and 70% (UWB1.289, p < 0.05) in cells transfected with si*UCA1*.

(F) *UCA1* overexpression in OSEC4C2 cells increases nuclear YAP. OSEC4C2 control cells and OSEC4C2 cells with *UCA1* overexpression were fractionated into Cy and Nu fractions and blotted for β-tubulin, U1-70k, and YAP. Nuclear YAP is elevated 30% (p < 0.05).

(G) *UCA1* facilitates AMOTp130 binding to YAP. High-grade serous EOC cell lines were transfected with siCtrl or si*UCA1* for 72 h. Co-immunoprecipitation experiments were performed using an anti-YAP antibody. Retrieval of AMOT is reduced 70% (CaOV3, p < 0.05) and 50% (UWB1.289, p < 0.05) in cells transfected with si*UCA1*.

(H) Working model for AMOT-mediated activation of YAP and target genes by *UCA1*.

SE, super-enhancer. ImageJ was used for quantification of proteins in (A, C, E, F, and G) from three independent replicates. Data shown in (B and D) are mean ± SD from three independent experiments. *p < 0.05, **p < 0.01, ***p < 0.001, ns, not significant, Student's t test. See also Figure S4.

activation of YAP target genes was dampened (Figure 6A), indicating that AMOT mediates the activation of YAP target genes by *UCA1*.

When phosphorylated at Ser127, YAP protein is retained in the cytoplasm and downstream signaling is repressed (Zhao et al., 2010). When total YAP protein levels are constant, increased YAPpS127 should result in reduced nuclear YAP. We therefore compared nuclear YAP expression between control and *UCA1* KO cells using cellular fractionation. Successful fractionation of the OVCA429 KO model was verified using cytoplasmic protein marker β-tubulin and nuclear protein marker U1-70k (Figure 6C) as well as cytoplasmic RNA marker *18S* rRNA and nuclear RNA marker *U6* snRNA (Figure S4A). These data show that *UCA1* predominantly localizes to the cytoplasm (∼94% on average, Figure S4A). Nuclear YAP expression decreased ∼2-fold in *UCA1* KO cells (KO-1 and KO-2) compared with WT cells (Ctrl 1 and Ctrl 2) (p = 3×10^{-4}) (Figures 6C and 6D). In addition, fractionation experiments were performed in three ovarian cancer cell lines following *UCA1* KD. Similarly, nuclear YAP was reduced 2-fold in *UCA1* KD CaOV3 and 3-fold in *UCA1* KD UWB1.289 cells compared with control siCtrl-treated cells (p = 0.014 and p = 0.006, respectively) (Figure 6E). Fractionation experiments were also conducted in OSEC4C2 cells overexpressing with control vector or *UCA1* (Figures 6F and S4B). Predominant cytoplasmic expression *UCA1* was confirmed in OSEC4C2 cells overexpressing *UCA1* (Figure S4B) and nuclear YAP was increased (Figure 6F). These data indicate that cytoplasmic *UCA1* activates YAP target genes *via* dephosphorylation and nuclear translocation of YAP.

Since *UCA1* KD affects neither AMOT protein expression (Figure 6A) nor localization (Figure 6E), we tested whether *UCA1* affects the AMOT-YAP interaction. Two-fold less AMOTp130 coimmunoprecipitated with YAP when *UCA1* was depleted (Figure 6G), evidence that *UCA1* promotes AMOTp130-YAP interaction. In summary, we propose a model in which cytoplasmic *UCA1* binds to AMOT to facilitate an interaction between AMOT and YAP, which prevents the pLATS1/2-YAP interaction and YAP phosphorylation. The net result is a larger pool of active YAP, which relocates to the activate YAP target genes (Figure 6H).

DISCUSSION

UCA1 is conserved in primates and expressed highly in the early embryo but not in most adult tissues (Wang et al., 2008). Originally *UCA1* was found to be overexpressed in bladder carcinoma (Wang et al., 2006) and was later shown to be upregulated in many other malignancies (Chen et al., 2016; Fang et al., 2014; Han et al., 2014; Hughes et al., 2015; Li et al., 2014, 2016a, 2016b; Na et al., 2015; Nie et al., 2016; Tian et al., 2014; Tuo et al., 2015; Wang et al., 2015; Zhang et al., 2016; Zhao et al., 2017; Zheng et al., 2015). Multiple underlying mechanisms have been proposed to explain the pro-oncogenic effects of *UCA1*, including inhibition of p27 (Han et al., 2014), activation of Wnt/β-Catenin signaling (Yang et al., 2016), promotion of KLF4-KRT6/13 signaling (Na et al., 2015), or function as miRNA sponge (Bian et al., 2016; Fang et al., 2017; He et al., 2017; Li et al., 2015, 2017, 2018; Lu et al., 2017; Nie et al., 2016; Sun et al., 2018; Tian et al., 2018; Tuo et al., 2015; Wang et al., 2015; Wu and Zhou, 2018; Xiao et al., 2017;

Xue et al., 2016; Zhang et al., 2017; Zhou et al., 2018, 2017; Zhu et al., 2018). However, the mechanistic pathways directly regulated by *UCA1* are unclear.

In our study, we found that *UCA1* overexpression drives ovarian cancer development. Our functional proteomic analyses of *UCA1* KO models revealed that *UCA1* activates YAP and its target genes, which may account for *UCA1*'s tumor growth promotion phenotype. To dissect the underlying mechanism of how *UCA1* activates YAP and its target gens, iRAP was performed and revealed that *UCA1* directly interacts with AMOTp130. AMOT was initially reported as a negative regulator of YAP *via* cytoplasmic retention of YAP protein (Zhao et al., 2011). However, more recent evidence suggests that AMOT can both negatively (Chan et al., 2011; Dai et al., 2013; Paramasivam et al., 2011; Wang et al., 2011) and positively regulate (Lv et al., 2016; Yi et al., 2013) YAP. In the present study, we demonstrated that AMOT is a positive regulator of YAP and its targets genes in ovarian cancer. In the cytoplasm of EOC cells, overexpressed *UCA1* enhances the interaction between AMOTp130 and YAP. This may be due to a conformational change of AMOTp130 induced by *UCA1* binding; alternatively, *UCA1* may affect the phosphorylation of AMOTp130, which in turn regulates AMOTp130-YAP interaction and subcellular localization of the complex (Dai et al., 2013; Moleirinho et al., 2017). However, the latter situation is unlikely as *UCA1* does not affect AMOT localization in EOC (Figure 6E). The enhanced AMOTp130-YAP interaction is therefore more likely to antagonize the pLATS1/2-YAP interaction that leads to phosphorylation of YAP (Yi et al., 2013) since overlapping regions of YAP bind to AMOT or LATS1/2 (Hao et al., 2008; Zhao et al., 2011). The indirect impact of *UCA1* is therefore dephosphorylation of YAP, which in turn promotes nuclear translocation of YAP and facilitates its binding to TEAD to activate expression of a pro-oncogenic gene signature.

In the current study, we develop a strategy LncRNA Interpreter to prioritize and then functionally dissect candidate lncRNAs in cancer. Using this approach, we reveal *UCA1* as a super-enhancer-regulated lncRNA in EOC and an unconventional lncRNA regulator of Hippo-YAP signaling and characterize a critical function for *UCA1* in the activation of YAP and its target genes in EOC. Our data implicate the *UCA1*-AMOTp130-YAP signaling axis in the development of EOC that may represent a potential target for therapeutic intervention. More broadly, this proof-of-concept study demonstrates that the protein-centric LncRNA Interpreter strategy can be readily applied to efficiently elucidate the functional role of other lncRNAs implicated in complex diseases.

Limitations of the Study

In this study, we demonstrated that *UCA1* activates the transcription coactivator YAP and its target genes in both gain-of-function and loss-of-function experiments. It is plausible that *UCA1* prevents YAP phosphorylation by pLATS1/2, but direct evidence for this is missing owing to the low expression of LATS1/2 in our models. Future studies evaluating YAP and AMOTp130 post-transcriptional modifications would likely yield a deeper mechanistic insight into the regulation of Hippo-YAP signaling pathway by *UCA1*.

METHODS

All methods can be found in the accompanying Transparent Methods supplemental file.

SUPPLEMENTAL INFORMATION

Supplemental Information can be found online at https://doi.org/10.1016/j.isci.2019.06.025.

ACKNOWLEDGMENTS

iScience

CellPress

AUTHOR CONTRIBUTIONS

DECLARATION OF INTERESTS

REFERENCES

Bian, Z., Jin, L., Zhang, J., Yin, Y., Quan, C., Hu, Y., Feng, Y., Liu, H., Fei, B., Mao, Y., et al. (2016). LncRNA-UCA1 enhances cell proliferation and 5-fluorouracil resistance in colorectal cancer by inhibiting miR-204-5p. Sci. Rep. 6, 23892.

Calin, G.A., Liu, C.G., Ferracin, M., Hyslop, T., Spizzo, R., Sevignani, C., Fabbri, M., Cimmino, A., Lee, E.J., Wojcik, S.E., et al. (2007). Ultraconserved regions encoding ncRNAs are altered in human leukemias and carcinomas. Cancer Cell 12, 215–229.

Cancer Genome Atlas Research Network. (2011). Integrated genomic analyses of ovarian carcinoma. Nature 474, 609–615.

Chan, S.W., Lim, C.J., Chong, Y.F., Pobbati, A.V., Huang, C., and Hong, W. (2011). Hippo pathway-independent restriction of TAZ and YAP by angiomotin. J. Biol. Chem. 286, 7018–7026.

Charboneau, L., Tory, H., Chen, T., Winters, M., Petricoin, E.F., 3rd, Liotta, L.A., and Paweletz, C.P. (2002). Utility of reverse phase protein arrays: applications to signalling pathways and human body arrays. Brief. Funct. Genomic. Proteomic. 1, 305–315.

Chen, P., Wan, D., Zheng, D., Zheng, Q., Wu, F., and Zhi, Q. (2016). Long non-coding RNA UCA1 promotes the tumorigenesis in pancreatic cancer. Biomed. Pharmacother. 83, 1220–1226.

Chu, C., Zhang, Q.C., da Rocha, S.T., Flynn, R.A., Bharadwaj, M., Calabrese, J.M., Magnuson, T., Heard, E., and Chang, H.Y. (2015). Systematic discovery of Xist RNA binding proteins. Cell 161, 404–416.

Dai, X., She, P., Chi, F., Feng, Y., Liu, H., Jin, D., Zhao, Y., Guo, X., Jiang, D., Guan, K.L., et al. (2013). Phosphorylation of angiomotin by Lats1/2 kinases inhibits F-actin binding, cell migration, and angiogenesis. J. Biol. Chem. 288, 34041–34051.

Derrien, T., Johnson, R., Bussotti, G., Tanzer, A., Djebali, S., Tilgner, H., Guernec, G., Martin, D., Merkel, A., Knowles, D.G., et al. (2012). The GENCODE v7 catalog of human long noncoding RNAs: analysis of their gene structure, evolution, and expression. Genome Res. 22, 1775–1789.

Ernkvist, M., Aase, K., Ukomadu, C., Wohlschlegel, J., Blackman, R., Veitonmaki, N.,

Bratt, A., Dutta, A., and Holmgren, L. (2006). p130-angiomotin associates to actin and controls endothelial cell shape. FEBS J. 273, 2000–2011.

Ernkvist, M., Birot, O., Sinha, I., Veitonmaki, N., Nystrom, S., Aase, K., and Holmgren, L. (2008). Differential roles of p80- and p130-angiomotin in the switch between migration and stabilization of endothelial cells. Biochim. Biophys. Acta 1783, 429–437.

Fang, Z., Wu, L., Wang, L., Yang, Y., Meng, Y., and Yang, H. (2014). Increased expression of the long non-coding RNA UCA1 in tongue squamous cell carcinomas: a possible correlation with cancer metastasis. Oral Surg. Oral Med. Oral Pathol. Oral Radiol. 117, 89–95.

Fang, Z., Zhao, J., Xie, W., Sun, Q., Wang, H., and Qiao, B. (2017). LncRNA UCA1 promotes proliferation and cisplatin resistance of oral squamous cell carcinoma by suppressing miR-184 expression. Cancer Med. 6, 2897–2908.

Filippakopoulos, P., Qi, J., Picaud, S., Shen, Y., Smith, W.B., Fedorov, O., Morse, E.M., Keates, T., Hickman, T.T., Felletar, I., et al. (2010). Selective inhibition of BET bromodomains. Nature 468, 1067–1073.

Gupta, R.A., Shah, N., Wang, K.C., Kim, J., Horlings, H.M., Wong, D.J., Tsai, M.C., Hung, T., Argani, P., Rinn, J.L., et al. (2010). Long non-coding RNA HOTAIR reprograms chromatin state to promote cancer metastasis. Nature 464, 1071–1076.

Guttman, M., Amit, I., Garber, M., French, C., Lin, M.F., Feldser, D., Huarte, M., Zuk, O., Carey, B.W., Cassady, J.P., et al. (2009). Chromatin signature reveals over a thousand highly conserved large non-coding RNAs in mammals. Nature 458, 223–227.

Guttman, M., Garber, M., Levin, J.Z., Donaghey, J., Robinson, J., Adiconis, X., Fan, L., Koziol, M.J., Gnirke, A., Nusbaum, C., et al. (2010). Ab initio reconstruction of cell type-specific transcriptomes in mouse reveals the conserved multi-exonic structure of lincRNAs. Nat. Biotechnol. 28, 503–510.

Guttman, M., and Rinn, J.L. (2012). Modular regulatory principles of large non-coding RNAs. Nature 482, 339–346.

Han, Y., Yang, Y.N., Yuan, H.H., Zhang, T.T., Sui, H., Wei, X.L., Liu, L., Huang, P., Zhang, W.J., and Bai, Y.X. (2014). UCA1, a long non-coding RNA up-regulated in colorectal cancer influences cell proliferation, apoptosis and cell cycle distribution. Pathology 46, 396–401.

Hao, Y., Chun, A., Cheung, K., Rashidi, B., and Yang, X. (2008). Tumor suppressor LATS1 is a negative regulator of oncogene YAP. J. Biol. Chem. 283, 5496–5509.

He, Z., Wang, Y., Huang, G., Wang, Q., Zhao, D., and Chen, L. (2017). The lncRNA UCA1 interacts with miR-182 to modulate glioma proliferation and migration by targeting iASPP. Arch. Biochem. Biophys. 623–624, 1–8.

Hughes, J.M., Legnini, I., Salvatori, B., Masciarelli, S., Marchioni, M., Fazi, F., Morlando, M., Bozzoni, I., and Fatica, A. (2015). C/EBPalpha-p30 protein induces expression of the oncogenic long non-coding RNA UCA1 in acute myeloid leukemia. Oncotarget 6, 18534–18544.

Jiang, Y., Jiang, Y.-Y., Xie, J.-J., Mayakonda, A., Hazawa, M., Chen, L., Xiao, J.-F., Li, C.-Q., Huang, M.-L., Ding, L.-W., et al. (2018). Co-activation of super-enhancer-driven CCAT1 by TP63 and SOX2 promotes squamous cancer progression. Nat. Commun. 9, 3619.

Kotake, Y., Nakagawa, T., Kitagawa, K., Suzuki, S., Liu, N., Kitagawa, M., and Xiong, Y. (2011). Long non-coding RNA ANRIL is required for the PRC2 recruitment to and silencing of p15(INK4B) tumor suppressor gene. Oncogene 30, 1956–1962.

Kretz, M., Webster, D.E., Flockhart, R.J., Lee, C.S., Zehnder, A., Lopez-Pajares, V., Qu, K., Zheng, G.X., Chow, J., Kim, G.E., et al. (2012). Suppression of progenitor differentiation requires the long noncoding RNA ANCR. Genes Dev. 26, 338–343.

Li, D., Li, H., Yang, Y., and Kang, L. (2018). Long noncoding RNA urothelial carcinoma associated 1 promotes the proliferation and metastasis of human lung tumor cells by regulating MicroRNA-144. Oncol. Res. https://doi.org/10.3727/096504017X15009792179602.

Li, H.J., Li, X., Pang, H., Pan, J.J., Xie, X.J., and Chen, W. (2015). Long non-coding RNA UCA1 promotes glutamine metabolism by targeting

miR-16 in human bladder cancer. Jpn. J. Clin. Oncol. 45, 1055–1063.

Li, H.J., Sun, X.M., Li, Z.K., Yin, Q.W., Pang, H., Pan, J.J., Li, X., and Chen, W. (2017). LncRNA UCA1 promotes mitochondrial function of bladder cancer via the MiR-195/ARL2 signaling pathway. Cell. Physiol. Biochem. 43, 2548–2561.

Li, J.Y., Ma, X., and Zhang, C.B. (2014). Overexpression of long non-coding RNA UCA1 predicts a poor prognosis in patients with esophageal squamous cell carcinoma. Int. J. Clin. Exp. Pathol. 7, 7938–7944.

Li, W., Xie, P., and Ruan, W.H. (2016a). Overexpression of lncRNA UCA1 promotes osteosarcoma progression and correlates with poor prognosis. J. Bone Oncol. 5, 80–85.

Li, Y., Wang, T., Li, Y., Chen, D., Yu, Z., Jin, L., Ni, L., Yang, S., Mao, X., Gui, Y., and Lai, Y. (2016b). Identification of long-non coding RNA UCA1 as an oncogene in renal cell carcinoma. Mol. Med. Rep. 13, 3326–3334.

Loewer, S., Cabili, M.N., Guttman, M., Loh, Y.H., Thomas, K., Park, I.H., Garber, M., Curran, M., Onder, T., Agarwal, S., et al. (2010). Large intergenic non-coding RNA-RoR modulates reprogramming of human induced pluripotent stem cells. Nat. Genet. 42, 1113–1117.

Lovén, J., Hoke, H.A., Lin, C.Y., Lau, A., Orlando, D.A., Vakoc, C.R., Bradner, J.E., Lee, T.I., and Young, R.A. (2013). Selective inhibition of tumor oncogenes by disruption of super-enhancers. Cell 153, 320–334.

Lu, Y., Liu, W.G., Lu, J.H., Liu, Z.J., Li, H.B., Liu, G.J., She, H.Y., Li, G.Y., and Shi, X.H. (2017). LncRNA UCA1 promotes renal cell carcinoma proliferation through epigenetically repressing p21 expression and negatively regulating miR-495. Tumour Biol. 39, 1010428317701632.

Lv, M., Li, S., Luo, C., Zhang, X., Shen, Y., Sui, Y.X., Wang, F., Wang, X., Yang, J., Liu, P., and Yang, J. (2016). Angiomotin promotes renal epithelial and carcinoma cell proliferation by retaining the nuclear YAP. Oncotarget 7, 12393–12403.

Matallanas, D., Romano, D., Yee, K., Meissl, K., Kucerova, L., Piazzolla, D., Baccarini, M., Vass, J.K., Kolch, W., and O'Neill, E. (2007). RASSF1A elicits apoptosis through an MST2 pathway directing proapoptotic transcription by the p73 tumor suppressor protein. Mol. Cell 27, 962–975.

McHugh, C.A., Chen, C.K., Chow, A., Surka, C.F., Tran, C., McDonel, P., Pandya-Jones, A., Blanco, M., Burghard, C., Moradian, A., et al. (2015). The Xist lncRNA interacts directly with SHARP to silence transcription through HDAC3. Nature 521, 232–236.

Minajigi, A., Froberg, J., Wei, C., Sunwoo, H., Kesner, B., Colognori, D., Lessing, D., Payer, B., Boukhali, M., Haas, W., and Lee, J.T. (2015). Chromosomes. A comprehensive Xist interactome reveals cohesin repulsion and an RNA-directed chromosome conformation. Science 349, https://doi.org/10.1126/science.aab2276.

Mitra, R., Chen, X., Greenawalt, E.J., Maulik, U., Jiang, W., Zhao, Z., and Eischen, C.M. (2017). Decoding critical long non-coding RNA in ovarian

cancer epithelial-to-mesenchymal transition. Nat. Commun. 8, 1604.

Moleirinho, S., Hoxha, S., Mandati, V., Curtale, G., Troutman, S., Ehmer, U., and Kissil, J.L. (2017). Regulation of localization and function of the transcriptional co-activator YAP by angiomotin. Elife 6, https://doi.org/10.7554/eLife.23966.

Na, X.Y., Liu, Z.Y., Ren, P.P., Yu, R., and Shang, X.S. (2015). Long non-coding RNA UCA1 contributes to the progression of prostate cancer and regulates proliferation through KLF4-KRT6/13 signaling pathway. Int. J. Clin. Exp. Med. 8, 12609–12616.

Nie, W., Ge, H.J., Yang, X.Q., Sun, X., Huang, H., Tao, X., Chen, W.S., and Li, B. (2016). LncRNA-UCA1 exerts oncogenic functions in non-small cell lung cancer by targeting miR-193a-3p. Cancer Lett. 371, 99–106.

Paramasivam, M., Sarkeshik, A., Yates, J.R., 3rd, Fernandes, M.J., and McCollum, D. (2011). Angiomotin family proteins are novel activators of the LATS2 kinase tumor suppressor. Mol. Biol. Cell 22, 3725–3733.

Patrie, K.M. (2005). Identification and characterization of a novel tight junction-associated family of proteins that interacts with a WW domain of MAGI-1. Biochim. Biophys. Acta 1745, 131–144.

Paweletz, C.P., Charboneau, L., Bichsel, V.E., Simone, N.L., Chen, T., Gillespie, J.W., Emmert-Buck, M.R., Roth, M.J., Petricoin, I.E., and Liotta, L.A. (2001). Reverse phase protein microarrays which capture disease progression show activation of pro-survival pathways at the cancer invasion front. Oncogene 20, 1981–1989.

Peng, L., Jiang, B., Yuan, X., Qiu, Y., Peng, J., Huang, Y., Zhang, C., Zhang, Y., Lin, Z., Li, J., et al. (2019). Super-enhancer-associated long noncoding RNA HCCL5 is activated by ZEB1 and promotes the malignancy of hepatocellular carcinoma. Cancer Res. 79, 572–584.

Qiu, J.J., Lin, Y.Y., Ye, L.C., Ding, J.X., Feng, W.W., Jin, H.Y., Zhang, Y., Li, Q., and Hua, K.Q. (2014). Overexpression of long non-coding RNA HOTAIR predicts poor patient prognosis and promotes tumor metastasis in epithelial ovarian cancer. Gynecol. Oncol. 134, 121–128.

Robinson, M.D., and Oshlack, A. (2010). A scaling normalization method for differential expression analysis of RNA-seq data. Genome Biol. 11, R25.

Siegel, R.L., Miller, K.D., and Jemal, A. (2016). Cancer statistics, 2016. CA Cancer J. Clin. 66, 7–30.

Sowa, M.E., Bennett, E.J., Gygi, S.P., and Harper, J.W. (2009). Defining the human deubiquitinating enzyme interaction landscape. Cell 138, 389–403.

Sun, M.D., Zheng, Y.Q., Wang, L.P., Zhao, H.T., and Yang, S. (2018). Long noncoding RNA UCA1 promotes cell proliferation, migration and invasion of human leukemia cells via sponging miR-126. Eur. Rev. Med. Pharmacol. Sci. 22, 2233–2245.

Tanos, V., Prus, D., Ayesh, S., Weinstein, D., Tykocinski, M.L., De-Groot, N., Hochberg, A., and Ariel, I. (1999). Expression of the imprinted H19

oncofetal RNA in epithelial ovarian cancer. Eur. J. Obstet. Gynecol. Reprod. Biol. 85, 7–11.

Tian, S., Yuan, Y., Li, Z., Gao, M., Lu, Y., and Gao, H. (2018). LncRNA UCA1 sponges miR-26a to regulate the migration and proliferation of vascular smooth muscle cells. Gene. https://doi.org/10.1016/j.gene.2018.06.031.

Tian, Y., Zhang, X., Hao, Y., Fang, Z., and He, Y. (2014). Potential roles of abnormally expressed long noncoding RNA UCA1 and Malat-1 in metastasis of melanoma. Melanoma Res. 24, 335–341.

Tuo, Y.L., Li, X.M., and Luo, J. (2015). Long noncoding RNA UCA1 modulates breast cancer cell growth and apoptosis through decreasing tumor suppressive miR-143. Eur. Rev. Med. Pharmacol. Sci. 19, 3403–3411.

Wang, F., Li, X., Xie, X., Zhao, L., and Chen, W. (2008). UCA1, a non-protein-coding RNA up-regulated in bladder carcinoma and embryo, influencing cell growth and promoting invasion. FEBS Lett. 582, 1919–1927.

Wang, F., Ying, H.Q., He, B.S., Pan, Y.Q., Deng, Q.W., Sun, H.L., Chen, J., Liu, X., and Wang, S.K. (2015). Upregulated lncRNA-UCA1 contributes to progression of hepatocellular carcinoma through inhibition of miR-216b and activation of FGFR1/ERK signaling pathway. Oncotarget 6, 7899–7917.

Wang, P., Ren, Z., and Sun, P. (2012). Overexpression of the long non-coding RNA MEG3 impairs in vitro glioma cell proliferation. J. Cell Biochem. 113, 1868–1874.

Wang, W., Huang, J., and Chen, J. (2011). Angiomotin-like proteins associate with and negatively regulate YAP1. J. Biol. Chem. 286, 4364–4370.

Wang, X.S., Zhang, Z., Wang, H.C., Cai, J.L., Xu, Q.W., Li, M.Q., Chen, Y.C., Qian, X.P., Lu, T.J., Yu, L.Z., et al. (2006). Rapid identification of UCA1 as a very sensitive and specific unique marker for human bladder carcinoma. Clin. Cancer Res. 12, 4851–4858.

Wu, H., and Zhou, C. (2018). Long non-coding RNA UCA1 promotes lung cancer cell proliferation and migration via microRNA-193a/HMGB1 axis. Biochem. Biophys. Res. Commun. 496, 738–745.

Xiao, J.N., Yan, T.H., Yu, R.M., Gao, Y., Zeng, W.L., Lu, S.W., Que, H.X., Liu, Z.P., and Jiang, J.H. (2017). Long noncoding RNA UCA1 regulates the expression of Snail2 by miR-203 to promote hepatocellular carcinoma progression. J. Cancer Res. Clin. Oncol. 143, 981–990.

Xie, J.-J., Jiang, Y.-Y., Jiang, Y., Li, C.-Q., Lim, M.-C., An, O., Mayakonda, A., Ding, L.-W., Long, L., Sun, C., et al. (2018). Super-enhancer-Driven long non-coding RNA LINC01503, regulated by TP63, is over-expressed and oncogenic in squamous cell carcinoma. Gastroenterology 154, 2137–2151.e1.

Xu, M.Z., Chan, S.W., Liu, A.M., Wong, K.F., Fan, S.T., Chen, J., Poon, R.T., Zender, L., Lowe, S.W., Hong, W., and Luk, J.M. (2011). AXL receptor kinase is a mediator of YAP-dependent oncogenic functions in hepatocellular carcinoma. Oncogene 30, 1229–1240.

Xue, M., Pang, H., Li, X., Li, H., Pan, J., and Chen, W. (2016). Long non-coding RNA urothelial cancer-associated 1 promotes bladder cancer cell migration and invasion by way of the hsa-miR-145-ZEB1/2-FSCN1 pathway. Cancer Sci. *107*, 18–27.

Yang, Y.T., Wang, Y.F., Lai, J.Y., Shen, S.Y., Wang, F., Kong, J., Zhang, W., and Yang, H.Y. (2016). Long non-coding RNA UCA1 contributes to the progression of oral squamous cell carcinoma by regulating the WNT/beta-catenin signaling pathway. Cancer Sci. *107*, 1581–1589.

Yi, C., Shen, Z., Stemmer-Rachamimov, A., Dawany, N., Troutman, S., Showe, L.C., Liu, Q., Shimono, A., Sudol, M., Holmgren, L., et al. (2013). The p130 isoform of angiomotin is required for Yap-mediated hepatic epithelial cell proliferation and tumorigenesis. Sci. Signal. *6*, ra77.

Zhang, L., Cao, X., Zhang, L., Zhang, X., Sheng, H., and Tao, K. (2016). UCA1 overexpression predicts clinical outcome of patients with ovarian cancer receiving adjuvant chemotherapy. Cancer Chemother. Pharmacol. *77*, 629–634.

Zhang, X., Gao, F., Zhou, L., Wang, H., Shi, G., and Tan, X. (2017). UCA1 regulates the growth and metastasis of pancreatic cancer by sponging miR-135a. Oncol. Res. *25*, 1529–1541.

Zhao, B., Li, L., Lu, Q., Wang, L.H., Liu, C.Y., Lei, Q., and Guan, K.L. (2011). Angiomotin is a novel Hippo pathway component that inhibits YAP oncoprotein. Genes Dev. *25*, 51–63.

Zhao, B., Li, L., Tumaneng, K., Wang, C.Y., and Guan, K.L. (2010). A coordinated phosphorylation by Lats and CK1 regulates YAP stability through SCF(beta-TRCP). Genes Dev. *24*, 72–85.

Zhao, W., Sun, C., and Cui, Z. (2017). A long noncoding RNA UCA1 promotes proliferation and predicts poor prognosis in glioma. Clin. Transl Oncol. *19*, 735–741.

Zheng, Q., Wu, F., Dai, W.Y., Zheng, D.C., Zheng, C., Ye, H., Zhou, B., Chen, J.J., and Chen, P. (2015). Aberrant expression of UCA1 in gastric cancer and its clinical significance. Clin. Transl Oncol. *17*, 640–646.

Zheng, Y., Vertuani, S., Nystrom, S., Audebert, S., Meijer, I., Tegnebratt, T., Borg, J.P., Uhlen, P., Majumdar, A., and Holmgren, L. (2009). Angiomotin-like protein 1 controls endothelial polarity and junction stability during sprouting angiogenesis. Circ. Res. *105*, 260–270.

Zhou, G., Li, C., Feng, J., Zhang, J., and Fang, Y. (2018). lncRNA UCA1 is a novel regulator in cardiomyocyte hypertrophy through targeting the miR-184/HOXA9 Axis. Cardiorenal Med. *8*, 130–139.

Zhou, Y., Wang, X., Zhang, J., He, A., Wang, Y.L., Han, K., Su, Y., Yin, J., Lv, X., and Hu, H. (2017). Artesunate suppresses the viability and mobility of prostate cancer cells through UCA1, the sponge of miR-184. Oncotarget *8*, 18260–18270.

Zhu, H.Y., Bai, W.D., Ye, X.M., Yang, A.G., and Jia, L.T. (2018). Long non-coding RNA UCA1 desensitizes breast cancer cells to trastuzumab by impeding miR-18a repression of Yes-associated protein 1. Biochem. Biophys. Res. Commun. *496*, 1308–1313.

Supplemental Information

Super-Enhancer-Associated LncRNA *UCA1*

Interacts Directly with AMOT to Activate

YAP Target Genes in Epithelial Ovarian Cancer

Xianzhi Lin, Tassja J. Spindler, Marcos Abraão de Souza Fonseca, Rosario I. Corona, Ji-Heui Seo, Felipe Segato Dezem, Lewyn Li, Janet M. Lee, Henry W. Long, Thomas A. Sellers, Beth Y. Karlan, Houtan Noushmehr, Matthew L. Freedman, Simon A. Gayther, and Kate Lawrenson

A

Super-enhancer

5kb

FTSEC (n=2)

OSEC (n=2)

CCOC (n=5)

EnOC (n=5)

HGSOC (n=5)

MOC (n=5)

H3K27ac Signal

$[^{510}_{0}$

OR10H1

B

Spearman's correlation
r = 0.47, *P* = 0.0427

OR10H1 (CPM)

Normalized Super-enhancer Signal

- CCOC
- EnOC
- HGSOC
- MOC
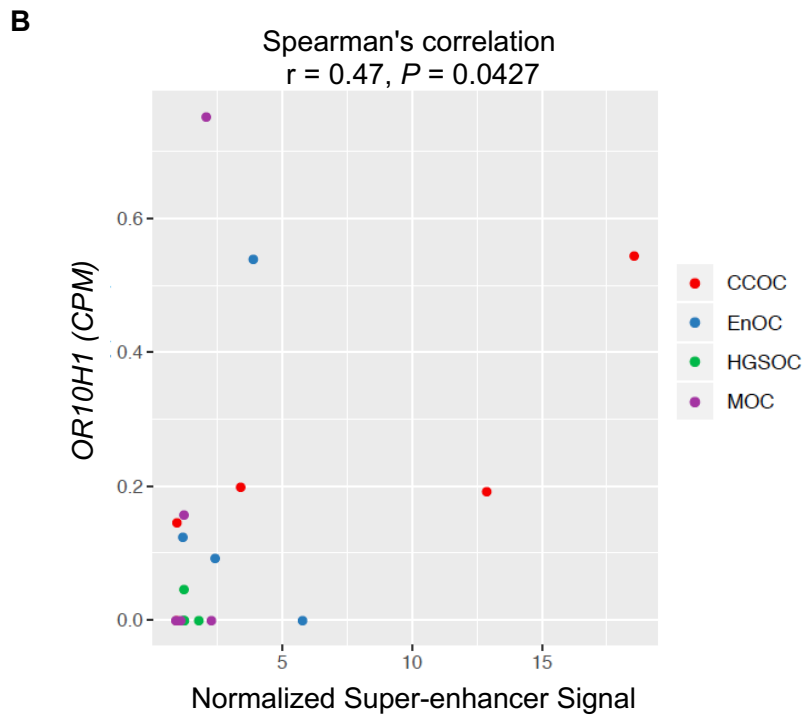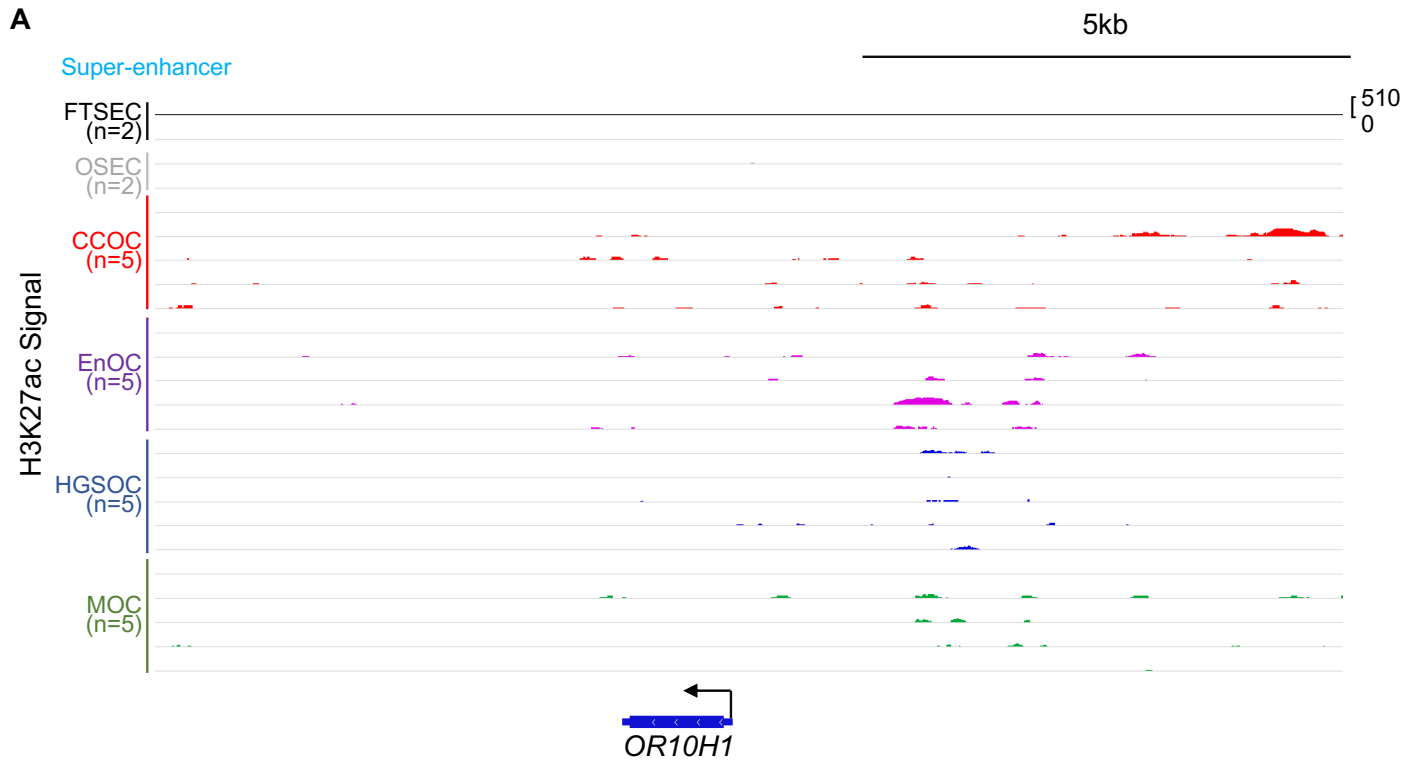
Figure S1. No evidence of super-enhancer activity at the *OR10H1* gene locus, Related to Figure 2

(A) H3K27ac signal at the *OR10H1* gene locus is shown at log scale. (B) Super-enhancer signals positively correlate with *OR10H1* expressions (Spearman's correlation, r=0.47, *P*=0.043). Counts per million (CPM) of *UCA1* from RNA-Seq is shown.
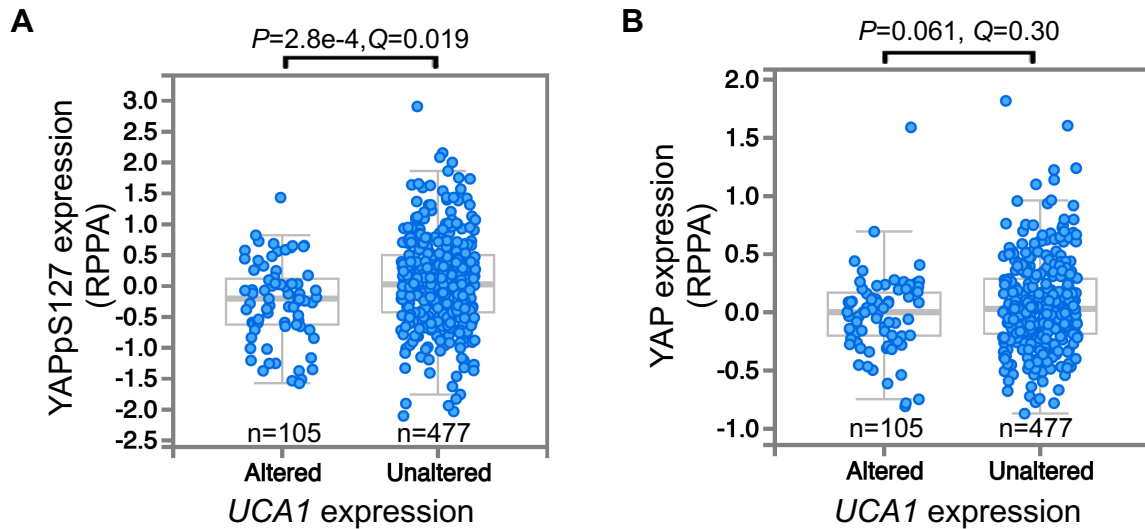
Figure S2. Overexpressed *UCA1* correlates with lower YAP phosphorylation in primary high-grade serous EOCs, Related to Figure 4A

(A) Comparison of RPPA data for YAPpS127 between ovarian cancers with (Altered) or without (Unaltered) *UCA1* amplification. (B) Total YAP is not significantly different between the two groups. Z-score threshold was set at 2. Data are from TCGA (http://www.cbioportal.org). *P*-value was determined using Student's *t*-test, while the *Q*-value was derived from Benjamini-Hochberg procedure.
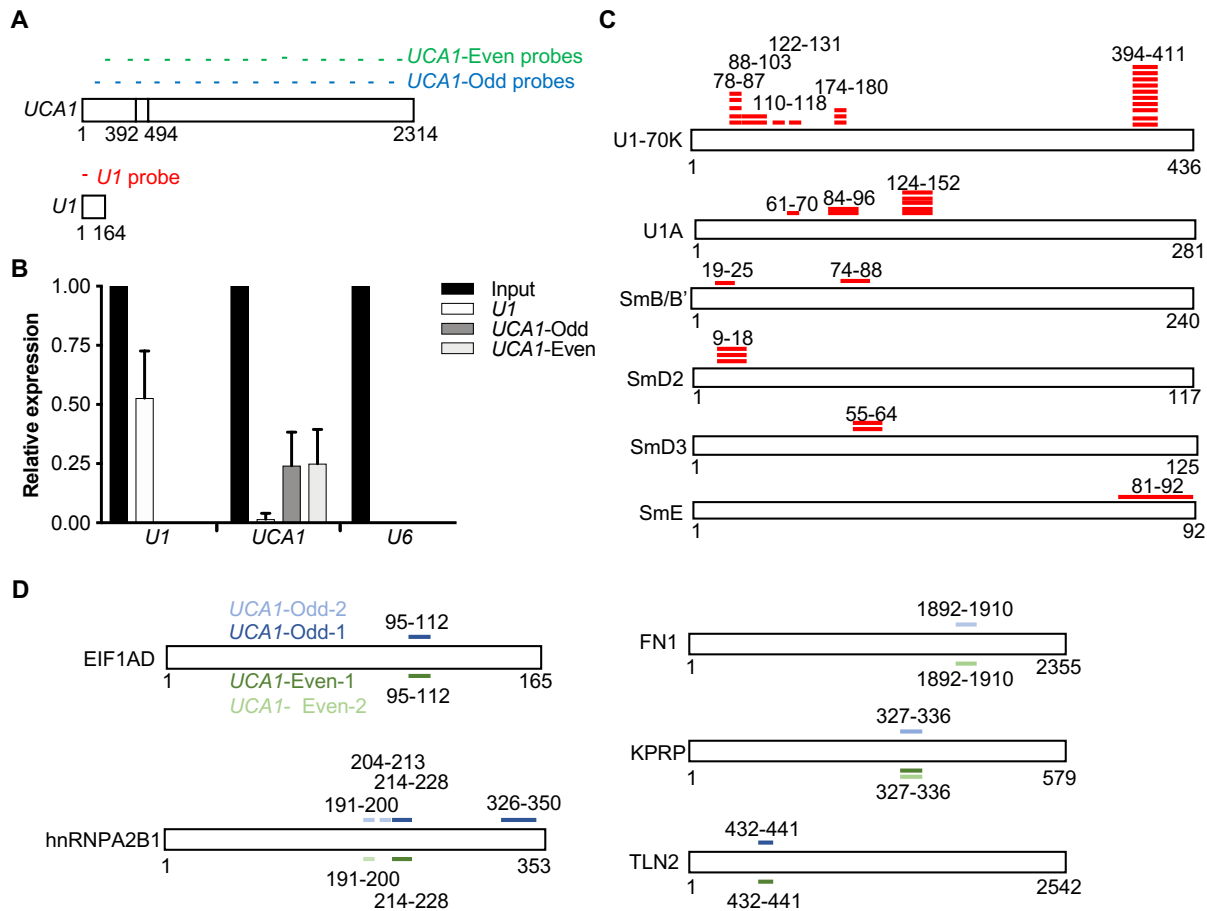
Figure S3. iRAP identifies the direct interacting proteome of *UCA1*, Related to Figure 5A

(A) Probe designing for *UCA1*-iRAP. Two sets of non-overlapping antisense DNA probes for *UCA1* were

designed and labeled with biotin at their 3' end. An antisense DNA probe complementary to 1-20 nt of *U1*

snRNA was included as a positive control. (B) RT-qPCR analysis of RNA retrieved from iRAP experiments.

Data shown are mean ± SD from 4 independent experiments. (C) Peptides were retrieved from *U1* iRAP-MS for

direct binding proteins of *U1* snRNA. Numbers indicate the starting amino acid position and the ending amino

acid position of the peptide retrieved or the full length of target protein. Protein length is not drawn in scale. (D)

The same peptides were reproducibly retrieved from *UCA1* iRAP-MS experiments. A selection of

representative proteins is shown. Numbers indicate the starting amino acid position and the ending amino acid

position of the peptide retrieved or the full length of target protein. Protein length is not drawn in scale. Data

shown are from 2 independent experiments.
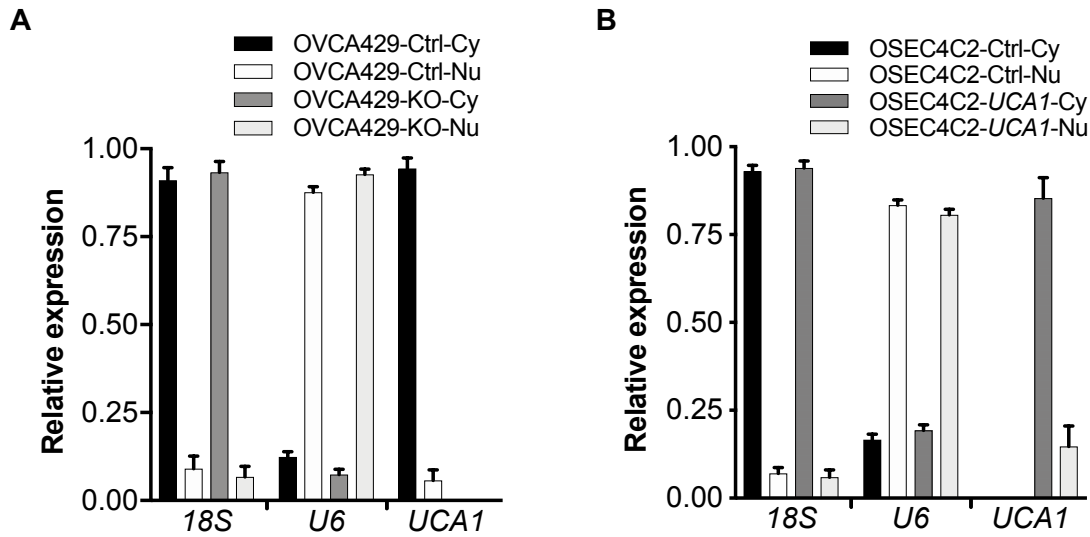
Figure S4. LncRNA *UCA1* predominantly localizes in cytoplasm, Related to Figure 6

(A) RT-qPCR measurement of cytoplasmic *18S* rRNA, nuclear *U6* snRNA and *UCA1* in OVCA429 fractionated samples. (B) RT-qPCR measurement of cytoplasmic *18S* rRNA, nuclear *U6* snRNA and *UCA1* in OSEC4C2 fractionated samples. Data shown are mean ± SD from 3 independent experiments.

Table S1. Prognostic lncRNAs in high-grade serous EOC, Related to Figure 2A

LncRNA Name	Importance-score	Raw-score	Chr	Start	End	Width	Strand	Gene Type
TTTY14	1.06572E+13	1.723	chrY	18872501	19077416	204916	-	lincRNA
PSMB1	99159107045	2.907	chr6	170535117	170553341	18225	-	protein_coding
ZFAS1	48072327683	2.585	chr20	49278178	49295738	17561	+	antisense
TUG1	40492304785	1.923	chr22	30970677	30979395	8719	+	antisense
FGD5-AS1	35063860805	2.147	chr3	14920347	14948424	28078	-	antisense
RP11-554D15.1	29197615843	-1.956	chr6	74069451	74690727	621277	+	lincRNA
CTB-55O6.12	23922544460	1.501	chr19	14137179	14171267	34089	+	antisense
GAS5	22959917722	3.715	chr1	173863900	173868882	4983	-	processed_transcript
RP5-1061H20.4	22563332287	2.269	chr1	229258281	229271028	12748	-	lincRNA
RP11-64D24.2	18447025405	2.552	chr11	114210616	114356571	145956	-	antisense
RP11-6N17.9	17963712426	1.799	chr17	47945424	47974438	29015	+	processed_transcript
OIP5-AS1	16976708028	2.315	chr15	41283990	41309737	25748	+	processed_transcript
SNHG15	16315350372	2.006	chr7	44983023	44986961	3939	-	lincRNA
RP11-865I6.2	15818503929	1.567	chr8	68848742	68852763	4022	-	lincRNA
ILF3-AS1	15338973685	1.479	chr19	10651862	10653844	1983	-	lincRNA
SNHG8	11732839093	2.472	chr4	118278709	118279823	1115	+	lincRNA
NOP14-AS1	11574773571	1.796	chr4	2934899	2961738	26840	+	antisense
LINC00662	11461006830	1.478	chr19	27684580	27793940	109361	-	lincRNA
AC005083.1	10597230777	2.135	chr7	20217577	20221700	4124	+	processed_transcript
LINC00648	10263227364	2.269	chr14	47764954	47795092	30139	-	lincRNA
AC004112.4	10158300092	2.129	chr7	112328189	112409623	81435	-	antisense
RP4-758J18.2	9884322048	1.601	chr1	1399522	1402046	2525	+	processed_transcript
RP11-38J22.3	9686546170	3.22	chr1	206117783	206126805	9023	+	antisense
RP11-458F8.4	7896100113	1.608	chr7	66902857	66906297	3441	+	lincRNA
SNHG9	7431812371	1.628	chr16	1964959	1965509	551	+	lincRNA
AJ006995.3	7240196117	-1.844	chr21	27954922	27985295	30374	+	lincRNA
LINC00339	6936706793	2.163	chr1	22024531	22031225	6695	+	lincRNA
LINC00578	6647351610	2.907	chr3	177441921	177752305	310385	+	lincRNA
RP11-47A8.5	6296575822	2.823	chr10	102642792	102644140	1349	-	lincRNA
SNHG17	6267686164	3.08	chr20	38420588	38435353	14766	-	processed_transcript
LINC00910	6258879085	2.145	chr17	43369845	43389199	19355	-	lincRNA
OSER1-AS1	6149104986	2.444	chr20	44210960	44226027	15068	+	lincRNA
C8orf31	6007255795	1.443	chr8	143039209	143059942	20734	+	processed_transcript
RP5-1132H15.1	5980054129	1.991	chr7	66119603	66165011	45409	-	antisense

RP11-430C7.4	5776440431	2.282	chr1	204603035	204616565	13531	+	antisense
RP11-191L9.4	5456541984	1.633	chr22	47631674	47855600	223927	+	lincRNA
RP11-115C21.2	5322360392	2.492	chr8	6403551	6407142	3592	-	antisense
RP11-296I10.3	5160521700	2.558	chr16	70156340	70173448	17109	-	antisense
UCA1	5062358192	1.923	chr19	15828961	15836320	7360	+	processed_transcript
RP11-799D4.4	5028502297	1.529	chr17	35231450	35242963	11514	-	antisense
RP11-526P5.2	4914956869	4.806	chr10	2501783	2567239	65457	+	lincRNA
LINC00284	4896454541	2.783	chr13	43908669	44030461	121793	+	lincRNA
FAM157C	-4806404688	2.891	chr16	90102271	90186204	83934	+	lincRNA
CTC-444N24.11	-5585259828	1.666	chr19	57304305	57308562	4258	+	lincRNA
C1orf132	-5802882217	1.689	chr1	207801518	207879096	77579	-	lincRNA
RMRP	-6118555929	1.777	chr9	35657751	35658018	268	-	lincRNA
RAD51-AS1	-7420839971	1.729	chr15	40686724	40695107	8384	-	processed_transcript
MIR205HG	-17249780561	1.462	chr1	209428820	209432838	4019	+	processed_transcript
RASSF8-AS1	-23114357641	2.725	chr12	25939329	25959765	20437	-	antisense
NEAT1	-29777169121	1.896	chr11	65422774	65445540	22767	+	lincRNA

Table S2. Super-enhancer-associated lncRNAs in high-grade serous EOCs, Related to Figure 2A

LncRNA Name	Chr	Start	End	Width	Strand	Gene Type
ZNF503-AS2	chr10	77160759	77168738	7980	+	processed_transcript
ZEB2-AS1	chr2	145275664	145279058	3395	+	antisense
ZBTB11-AS1	chr3	101395274	101398061	2788	+	antisense
WT1-AS	chr11	32457064	32480315	23252	+	antisense
UNC5B-AS1	chr10	72976981	72977985	1005	-	antisense
UCA1	chr19	15939771	15947130	7360	+	processed_transcript
UBXN8	chr8	30589764	30624522	34759	+	processed_transcript
TMPRSS4-AS1	chr11	117886487	117957508	71022	-	antisense
TMEM72-AS1	chr10	45306472	45455137	1E+05	-	antisense
THAP9-AS1	chr4	83814162	83822113	7952	-	antisense
TFAP2A-AS1	chr6	10409573	10416679	7107	+	antisense
STK4-AS1	chr20	43592435	43595043	2609	-	lincRNA
SSSCA1-AS1	chr11	65337131	65337744	614	-	antisense
SRP14-AS1	chr15	40331512	40359491	27980	+	lincRNA
SPPL2B	chr19	2328614	2355099	26486	+	processed_transcript
SNORA67	chr17	7476144	7485342	9199	+	processed_transcript
SNORA59B	chr17	19460524	19461224	701	+	sense_intronic
SNHG9	chr16	2014960	2015510	551	+	lincRNA
SNHG16	chr17	74553848	74561430	7583	+	processed_transcript
SNHG15	chr7	45022622	45026560	3939	-	lincRNA
SNHG10	chr14	95998634	96001209	2576	-	antisense
SNHG1	chr11	62619460	62623386	3927	-	processed_transcript
SNAI3-AS1	chr16	88729706	88753594	23889	+	antisense
SLC2A1-AS1	chr1	43424720	43449029	24310	+	lincRNA
SENP3-EIF4A1	chr17	7466604	7482033	15430	+	processed_transcript
SEMA3B	chr3	50304990	50314977	9988	+	processed_transcript
RPS10P7	chr1	201487831	201499602	11772	+	lincRNA
RNF157-AS1	chr17	74136637	74150731	14095	+	antisense
PTOV1-AS1	chr19	50341896	50354933	13038	-	antisense
PSMG3-AS1	chr7	1609709	1629262	19554	+	lincRNA
PROSER2-AS1	chr10	11891612	11936699	45088	-	antisense
PLAC4	chr21	42548249	42558715	10467	-	antisense
PDCD4-AS1	chr10	112629626	112631991	2366	-	antisense
PCOLCE-AS1	chr7	100187025	100201829	14805	-	antisense
PCED1B-AS1	chr12	47599681	47610239	10559	-	processed_transcript
PCBP1-AS1	chr2	70189395	70315978	1E+05	-	antisense
NEAT1	chr11	65190245	65213011	22767	+	lincRNA
MYLK-AS1	chr3	123304389	123363415	59027	+	antisense
MRPL23-AS1	chr11	2004467	2011150	6684	-	antisense
MIR29B1	chr7	130561495	130598069	36575	-	lincRNA
MIR22HG	chr17	1614805	1620468	5664	-	lincRNA
MIR210HG	chr11	565660	568457	2798	-	lincRNA
MIR194-2	chr11	64658827	64660921	2095	-	lincRNA
MIR142	chr17	56408245	56409869	1625	-	antisense
MIR10A	chr17	46656992	46659621	2630	-	sense_intronic
MEIS1-AS3	chr2	66653867	66660602	6736	-	antisense
MAP3K14-AS1	chr17	43325292	43345997	20706	+	antisense
MAP3K14	chr17	43340488	43394414	53927	-	processed_transcript
LMCD1-AS1	chr3	7994492	8653610	7E+05	-	antisense
LINC01011	chr6	2988201	2991407	3207	+	lincRNA
LINC01004	chr7	104590762	104653491	62730	-	antisense

LINC00974	chr17	39705858	39710747	4890	-	lincRNA
LINC00938	chr12	46119510	46121558	2049	-	lincRNA
LINC00899	chr22	46435787	46440733	4947	-	processed_transcript
LINC00857	chr10	81967466	81979413	11948	+	lincRNA
LINC00847	chr5	180257957	180262726	4770	+	lincRNA
LINC00638	chr14	105287538	105290055	2518	+	lincRNA
LINC00605	chr14	103653558	103655365	1808	-	lincRNA
LINC00518	chr6	10429488	10435107	5620	-	lincRNA
LINC00511	chr17	70319264	70636611	3E+05	-	lincRNA
LINC00336	chr6	33553883	33561115	7233	-	antisense
LINC00324	chr17	8123960	8127361	3402	-	lincRNA
LINC00319	chr21	44866481	44873773	7293	+	lincRNA
LINC00313	chr21	44881974	44899414	17441	-	lincRNA
LINC00176	chr20	62665697	62671315	5619	+	lincRNA
LINC00163	chr21	46409779	46414001	4223	-	lincRNA
LINC00114	chr21	40110945	40119384	8440	-	lincRNA
LINC00111	chr21	43099341	43117496	18156	+	lincRNA
KRTAP5-AS1	chr11	1592583	1620414	27832	+	antisense
ITGB2-AS1	chr21	46340966	46349593	8628	+	antisense
HPN-AS1	chr19	35549963	35597208	47246	-	antisense
HOXB-AS3	chr17	46626992	46683776	56785	+	antisense
HOXB-AS1	chr17	46620913	46628610	7698	+	antisense
HCG11	chr6	26522076	26526807	4732	+	lincRNA
GATA6-AS1	chr18	19746859	19748929	2071	-	lincRNA
FAM13A-AS1	chr4	89630940	89651254	20315	+	antisense
ENO1-AS1	chr1	8938894	8939953	1060	+	antisense
EMX2OS	chr10	119232726	119304579	71854	-	antisense
EGOT	chr3	4790876	4793274	2399	-	lincRNA
DLGAP1-AS1	chr18	3593730	3598350	4621	+	antisense
CYP1B1-AS1	chr2	38302791	38408997	1E+05	+	antisense
CSNK1G2-AS1	chr19	1952530	1954585	2056	-	antisense
CPEB2-AS1	chr4	14911585	15003669	92085	-	lincRNA
COL18A1-AS2	chr21	46827301	46829980	2680	-	antisense
COL18A1-AS1	chr21	46839631	46844985	5355	-	antisense
CDKN2B-AS1	chr9	21994777	22121096	1E+05	+	antisense
CD27-AS1	chr12	6548167	6560733	12567	-	antisense
BAIAP2-AS1	chr17	79002933	79008501	5569	-	lincRNA
ASB16-AS1	chr17	42253341	42264085	10745	-	antisense
ARHGAP26-AS1	chr5	142239169	142248487	9319	-	antisense
AGAP11	chr10	88752163	88769960	17798	+	processed_transcript
ACTN1-AS1	chr14	69446399	69454180	7782	+	antisense
ABO	chr9	136125788	136150617	24830	-	processed_transcript

Table S3. Differentially expressed proteins caused by disruption of *UCA1*, Related to Figure 4A

Protein	OVCA429-1	OVCA429-2	Control-1	Control-2	Control-3	*UCA1* KO1-1	*UCA1* KO1-2	*UCA1* KO1-3	*UCA1* KO2-1	*UCA1* KO2-2	Ratio (KO/WT)	T test
PEA-15-R-V_GBL1116480	1.04	1.03	1.06	1.07	1.09	0.94	0.91	0.97	0.97	0.97	0.90	9.10E-05
UGT1A-M-V_GBL1116415	1.12	1.11	1.05	1.11	1.13	0.93	0.91	0.89	0.97	0.98	0.85	1.66E-04
c-Met_pY1234_Y1235-R-V_GBL1115572	1.23	1.18	1.18	1.23	1.16	0.92	0.85	0.78	0.95	0.89	0.74	1.67E-04
Caveolin-1-R-V_GBL1115521	1.14	1.16	1.18	1.15	1.28	0.78	0.75	0.72	0.85	0.83	0.66	2.07E-04
H2AX_pS139-R-V_GBL1116473	1.02	1.03	1.04	1.02	1.00	0.97	0.98	0.98	0.97	0.98	0.95	9.14E-04
PCNA-M-C_GBL1116373	1.03	1.06	1.07	1.07	1.01	0.92	0.86	0.87	0.90	0.95	0.86	0.01
LDHA-R-C_GBL1115596	1.14	1.18	1.18	1.28	1.42	0.85	0.54	0.64	1.08	0.82	0.63	0.01
Rb_pS807_S811-R-V_GBL1115559	1.25	1.22	1.09	1.20	1.09	0.93	0.86	0.87	1.09	0.93	0.80	0.01
Bcl2A1-R-V_GBL1116330	1.11	1.04	1.11	1.00	1.03	0.98	0.93	0.95	0.95	0.96	0.90	0.01
MSH6-R-C_GBL1115609	1.08	1.07	1.11	1.10	1.14	0.90	0.78	0.82	1.04	0.93	0.81	0.01
Cyclin-B1-R-V_GBL1115524	1.07	1.10	1.05	1.07	1.03	1.01	1.00	0.95	0.88	0.83	0.88	0.01
PYGM-M-C_GBL1116395	1.07	1.09	1.01	1.08	1.10	0.98	0.86	0.86	1.02	0.90	0.86	0.01
Myosin-11-R-V_GBL1115630	1.01	1.18	0.92	1.27	1.28	0.85	0.50	0.54	1.05	0.79	0.66	0.01
CD49b-M-V_GBL1116425	0.97	0.99	0.95	1.12	1.04	0.94	0.84	0.88	1.04	0.96	0.92	0.02
Lck-R-V_GBL1115538	1.46	1.49	1.03	1.43	1.45	0.73	0.67	0.66	1.32	1.02	0.64	0.02
EGFR_pY1173-R-V_GBL1115526	1.10	1.07	1.10	0.98	1.02	0.93	0.96	0.90	0.95	0.93	0.89	0.02
Gys_pS641-R-V_GBL1115603	1.08	1.12	1.05	1.05	1.03	0.95	0.97	0.90	1.03	0.96	0.90	0.02
RBM15-R-V_GBL1115629	1.09	1.03	1.00	1.03	1.05	0.97	0.84	0.81	1.01	0.97	0.89	0.02
PMS2-R-V_GBL1116324	1.17	1.18	1.04	1.07	1.09	0.96	0.87	0.87	1.05	0.95	0.84	0.02
Src_pY416-R-C_GBL1116447	1.00	1.01	1.01	1.03	1.06	0.96	1.00	0.97	0.94	1.01	0.95	0.02
Transglutaminase-M-V_GBL1116383	0.87	0.96	1.11	1.05	1.09	0.51	0.55	0.56	0.95	0.96	0.69	0.02
XPA-M-V_GBL1116419	1.09	1.15	0.99	1.07	1.01	0.92	0.99	0.94	0.96	0.99	0.90	0.02
RPA32-T-C_GBL1116471	1.06	1.03	0.98	1.04	1.10	0.92	0.88	0.85	1.03	1.04	0.91	0.02
Ets-1-R-V_GBL1116361	1.24	1.18	1.36	1.01	1.24	0.95	0.69	0.73	0.99	0.90	0.70	0.03
Axl-R-V_GBL1116474	1.47	1.09	1.14	1.08	1.13	0.83	0.89	0.91	0.88	0.93	0.75	0.03
UQCRC2-M-C_GBL1116412	1.04	1.04	1.01	1.00	1.04	1.02	0.93	0.94	0.96	1.01	0.95	0.03
ERCC5-R-C_GBL1116336	1.00	1.00	1.08	1.07	1.06	0.99	0.96	0.94	0.93	0.98	0.92	0.04
S6_pS240_S244-R-V_GBL1115562	1.19	1.12	0.99	1.12	1.07	0.96	0.79	0.84	1.12	0.94	0.85	0.04
Glutaminase-R-C_GBL1116346	0.98	0.95	1.07	1.05	1.06	0.87	0.81	0.80	1.02	0.98	0.88	0.04
Rad50-M-V_GBL1116385	1.05	1.05	1.08	0.99	1.01	1.01	1.00	0.97	0.94	1.00	0.95	0.04
eEF2-R-C_GBL1115607	1.05	1.08	1.15	1.07	1.23	0.87	0.43	0.46	1.04	0.83	0.65	0.04
ERCC1-M-V_GBL1116435	1.03	1.08	0.96	1.03	1.02	0.93	0.93	0.93	1.00	0.99	0.93	0.04

Dvl3-R-V_GBL1116454	1.02	1.03	0.91	1.04	1.05	0.99	0.91	0.90	0.99	0.96	0.94	0.04
Myosin-IIa_pS1943-R-V_GBL1115635	1.23	1.43	1.02	1.28	1.50	0.82	0.17	0.26	1.30	0.90	0.54	0.05
FAK-R-C_GBL1115530	1.11	1.08	1.03	1.06	1.09	1.08	0.89	0.96	1.04	0.94	0.91	0.05
Chk1_pS296-R-V_GBL1116335	1.11	1.11	1.03	1.00	0.99	1.04	1.09	1.03	0.95	0.96	0.97	0.05
p53-R-C_GBL1115545	0.88	0.93	0.91	0.89	0.91	1.01	1.03	1.03	0.99	1.04	1.13	1.89E-04
NDRG1_pT346-R-V_GBL1116491	0.84	0.90	0.82	0.84	0.81	1.20	1.22	1.25	1.07	1.18	1.41	4.42E-04
Gab2-R-V_GBL1115594	0.88	0.91	0.82	0.80	0.80	1.06	1.05	1.05	0.93	0.99	1.20	7.12E-04
PDK1_pS241-R-V_GBL1115550	0.93	0.88	0.94	0.87	0.92	1.14	1.08	1.05	1.02	1.04	1.17	1.49E-03
Claudin-7-R-V_GBL1115586	0.85	0.86	0.82	0.99	0.98	1.06	1.32	1.16	1.45	1.32	1.40	1.52E-03
Tuberin_pT1462-R-V_GBL1116448	0.91	0.92	0.80	0.84	0.85	1.01	1.04	1.02	0.96	0.99	1.16	2.48E-03
INPP4b-R-V_GBL1115611	0.90	0.90	0.96	0.96	0.96	1.13	1.03	1.07	1.10	1.09	1.16	2.57E-03
p27_pT198-R-V_GBL1115587	0.97	0.95	1.00	0.94	0.95	1.01	1.03	1.04	0.99	0.98	1.05	2.92E-03
ACVRL1-R-C_GBL1116458	0.98	0.98	0.96	0.95	1.01	1.04	1.02	0.99	0.97	1.04	1.04	3.58E-03
Pdcd4-R-C_GBL1115583	0.85	0.89	0.88	0.93	0.97	1.02	1.07	1.09	1.04	1.04	1.17	4.02E-03
Tuberin-R-V_GBL1115566	0.96	0.95	0.88	0.98	0.97	1.14	1.04	1.02	1.08	1.04	1.12	4.51E-03
Caspase-3-R-C_GBL1115519	0.93	0.91	0.96	0.92	0.91	1.02	1.05	1.04	0.98	0.96	1.09	0.01
Tyro3-R-V_GBL1116457	0.95	0.96	0.93	0.92	0.93	1.04	1.06	1.00	0.99	1.11	1.11	0.01
c-Abl-R-V_GBL1116347	1.00	0.99	1.04	0.99	0.95	1.04	1.02	1.05	1.02	0.99	1.03	0.01
ER-R-V_GBL1116352	0.91	0.89	0.95	0.91	0.91	1.10	1.04	1.06	0.97	1.11	1.15	0.01
HER2-M-V_GBL1116406	0.92	0.92	0.93	0.91	0.95	1.04	1.06	1.03	0.94	1.06	1.11	0.01
A-Raf-R-V_GBL1116314	0.98	0.95	0.92	0.92	0.89	1.02	1.04	1.08	1.01	0.97	1.10	0.01
MMP2-R-V_GBL1115540	0.91	0.93	0.95	0.92	0.91	1.06	1.03	1.03	0.95	1.00	1.10	0.01
D-alpha-Tubulin-R-V_GBL1116339	1.01	0.98	0.94	0.91	0.93	1.14	1.05	1.04	0.96	0.97	1.08	0.01
CXCR4-R-C_GBL1116362	0.94	0.95	0.96	0.94	0.90	1.02	1.03	1.03	1.01	1.09	1.11	0.01
Cyclophilin-F-M-V_GBL1116413	0.92	0.97	0.91	0.93	0.90	1.03	1.02	1.04	0.96	1.01	1.09	0.01
P-Cadherin-R-C_GBL1116446	0.97	1.00	0.91	0.95	0.92	1.05	1.04	0.94	1.03	1.05	1.08	0.02
PDGFR-beta-R-V_GBL1116319	1.00	0.94	0.96	0.94	0.86	1.01	1.06	1.06	1.00	0.95	1.08	0.02
MEK2-R-V_GBL1116323	1.03	1.00	0.98	0.95	0.95	1.13	1.05	1.01	1.07	1.10	1.09	0.02
TFAM-R-V_GBL1116333	0.88	0.95	0.89	0.89	0.91	0.98	1.13	1.10	0.95	0.97	1.13	0.02
IGFBP5-G-C_GBL1116469	0.93	0.91	0.93	0.94	0.91	0.98	1.06	1.01	0.97	0.99	1.08	0.02
Bad_pS112-R-V_GBL1115511	1.00	0.88	1.01	0.89	0.94	1.14	1.11	1.06	1.06	0.99	1.14	0.02
Notch3-R-C_GBL1116354	0.89	0.88	0.99	0.94	0.97	1.02	1.06	1.04	1.00	1.03	1.10	0.02
mTOR_pS2448-R-C_GBL1115542	0.99	0.99	0.91	1.04	0.98	1.08	1.01	1.01	1.06	1.06	1.06	0.02
eIF4E-R-V_GBL1115571	0.88	0.92	1.01	0.95	0.98	0.98	0.98	1.05	0.99	1.00	1.05	0.02
MDM2_pS166-R-V_GBL1116306	0.96	0.94	1.00	1.01	1.01	1.09	1.02	1.01	1.08	1.07	1.07	0.02

Notch1-R-V_GBL1115610	0.99	1.02	0.91	0.89	0.91	1.08	1.03	1.03	1.08	1.03	1.11	0.03
ATM-R-V_GBL1116337	0.91	0.89	0.79	0.92	0.87	1.05	1.12	1.11	0.94	1.00	1.19	0.03
Rictor_pT1135-R-V_GBL1115627	0.93	0.92	0.90	0.99	0.91	1.04	1.03	1.03	0.98	0.98	1.09	0.03
Rictor-R-C_GBL1115626	0.95	0.94	0.92	0.97	0.94	1.03	1.03	1.04	0.97	0.98	1.07	0.04
Src-M-V_GBL1116378	1.01	0.93	0.93	0.88	0.81	1.04	1.13	0.99	1.02	1.11	1.16	0.04
YAP_pS127-R-E_GBL1115578	0.83	0.89	0.99	0.96	1.00	1.41	1.12	1.11	1.37	1.08	1.30	0.04
Puma-R-C_GBL1116329	0.89	0.92	0.91	0.91	0.90	1.01	1.02	1.04	1.30	1.01	1.18	0.04
Pdcd-1L1-G-C_GBL1116468	0.91	0.96	0.81	0.80	0.97	0.96	1.04	1.02	1.00	0.99	1.13	0.05
CD29-M-V_GBL1116426	0.89	0.93	0.96	0.95	0.95	0.95	1.06	1.02	0.94	1.02	1.07	0.05

The differentially expressed proteins with $P \leq 0.05$ are shown.

Table S4. iRAP antisense DNA probe sequences, Related to Figure 5

Target Sequence Access #	Probe Sequence	Length	Start	End	Gene ID	Gene Name	Note
NR_015379	GGACTCATTGTCCAGAAGAA	20	6	25	652995	*UCA1*	Odd
NR_015379	GTTATCTGTTGTCAGCAGAG	20	61	80	652995	*UCA1*	Odd
NR_015379	GAGATAGGAGAGGGGCAGCT	20	124	143	652995	*UCA1*	Odd
NR_015379	AAGCATGTCCGTATAGAAGA	20	231	250	652995	*UCA1*	Odd
NR_015379	ACGGAATGAGGGCCAGGACA	20	305	324	652995	*UCA1*	Odd
NR_015379	GAGGAGATCCGATTTGAAAT	20	381	400	652995	*UCA1*	Odd
NR_015379	TGGTCCAAGGGGCTTCTGAG	20	436	455	652995	*UCA1*	Odd
NR_015379	CAGCTAGGGTGTCTTCATAT	20	505	524	652995	*UCA1*	Odd
NR_015379	AATGACCGGGTAGGGTCTGG	20	579	598	652995	*UCA1*	Odd
NR_015379	TGGGCATGGCTTTATTCTGG	20	654	673	652995	*UCA1*	Odd
NR_015379	GTTTGTCTGATCGGCTCTCG	20	727	746	652995	*UCA1*	Odd
NR_015379	GCATGCTGGGATGGCCATTT	20	813	832	652995	*UCA1*	Odd
NR_015379	TTTTATAGGCGGCAGGTCTT	20	875	894	652995	*UCA1*	Odd
NR_015379	GACTTTTGACCCAGAGATTT	20	949	968	652995	*UCA1*	Odd
NR_015379	GTTGTCCATTTCATGAGAGT	20	1023	1042	652995	*UCA1*	Odd
NR_015379	CCCTCTAACAACAAACAACA	20	1111	1130	652995	*UCA1*	Odd
NR_015379	CTTTGTCTCCTGGATTAAGC	20	1161	1180	652995	*UCA1*	Odd
NR_015379	TCCCATAGGTGTGAGTGGCG	20	1249	1268	652995	*UCA1*	Odd
NR_015379	AGCCTTTTGTCCCCATTTTC	20	1320	1339	652995	*UCA1*	Odd
NR_015379	CAGTAATCAGGCATATTAGC	20	1399	1418	652995	*UCA1*	Odd
NR_015379	GCTAACAAGGTGCCAGTTAG	20	1467	1486	652995	*UCA1*	Odd
NR_015379	GACTGCGTGGACACCTTAAA	20	1541	1560	652995	*UCA1*	Odd
NR_015379	AGTTCCTTCTGGGGATTACT	20	1606	1625	652995	*UCA1*	Odd
NR_015379	GACGGATATGTGCAGGTCAC	20	1724	1743	652995	*UCA1*	Odd
NR_015379	CTGTTTCACTTCTTTGTGGT	20	1786	1805	652995	*UCA1*	Odd
NR_015379	CATAATGGTGGAATGTCGTA	20	1837	1856	652995	*UCA1*	Odd
NR_015379	GATGGGACTCATTGTCCAGG	20	1925	1944	652995	*UCA1*	Odd
NR_015379	TAGGCGTGGAAAGTTACAGT	20	2000	2019	652995	*UCA1*	Odd
NR_015379	CTGTTAATTCACTTGGGTGC	20	2089	2108	652995	*UCA1*	Odd
NR_015379	AGGTTCCTGTCACGCGTGTC	20	2151	2170	652995	*UCA1*	Odd
NR_015379	AGGTGCATGGTGGAGAGATG	20	29	48	652995	*UCA1*	Even
NR_015379	ATAGGGCTGGGGTAGGCTGT	20	102	121	652995	*UCA1*	Even
NR_015379	TGTTAATTCACTTGGGTGCA	20	178	197	652995	*UCA1*	Even

12

NR_015379	AGATTTTGGCACCAAGTGTC	20	251	270	652995	*UCA1*	Even
NR_015379	GGTCGCAGGTGGATCTCTTC	20	325	344	652995	*UCA1*	Even
NR_015379	CAGTCTTCAGCCACTAAGCC	20	401	420	652995	*UCA1*	Even
NR_015379	CCGTAAGAGTTACCCGAAGC	20	469	488	652995	*UCA1*	Even
NR_015379	GTTTGAGGGGTCAGACTTTT	20	542	561	652995	*UCA1*	Even
NR_015379	AGAGGGTCCTGCAGATGGAC	20	617	636	652995	*UCA1*	Even
NR_015379	GAAGAGGAGAGATCAAGCTG	20	683	702	652995	*UCA1*	Even
NR_015379	TGGAAGCATGGCCTTGGCTG	20	778	797	652995	*UCA1*	Even
NR_015379	AGGAACGGATGAAGCCTGCT	20	838	857	652995	*UCA1*	Even
NR_015379	GAGGATAGGGTCTCAAGATA	20	902	921	652995	*UCA1*	Even
NR_015379	ACCATGGGCAAGGATCTGAT	20	991	1010	652995	*UCA1*	Even
NR_015379	TGCCAAATATGTGGAACTGG	20	1060	1079	652995	*UCA1*	Even
NR_015379	GGCAAAGAGTGAAATGTCCC	20	1134	1153	652995	*UCA1*	Even
NR_015379	ATAGTTCTGATTGCAGATCC	20	1210	1229	652995	*UCA1*	Even
NR_015379	CCCTGTTGCTAAGCCGATGA	20	1282	1301	652995	*UCA1*	Even
NR_015379	GTAGGTGGCGATGAGTTTTT	20	1373	1392	652995	*UCA1*	Even
NR_015379	CTTGGAACTGCCCTAATAAA	20	1435	1454	652995	*UCA1*	Even
NR_015379	TCTAGTAAGTTTCGGGTCTA	20	1504	1523	652995	*UCA1*	Even
NR_015379	GCTGATATTTCTCCGGACTG	20	1578	1597	652995	*UCA1*	Even
NR_015379	CTTCAGCTCACAGGCCTGAC	20	1685	1704	652995	*UCA1*	Even
NR_015379	CTGCTCCAGACTTCTTGGCT	20	1759	1778	652995	*UCA1*	Even
NR_015379	GTGGGTTAATTAGTTAAGGC	20	1815	1834	652995	*UCA1*	Even
NR_015379	GATTGATCAGTTGGGGCAGG	20	1886	1905	652995	*UCA1*	Even
NR_015379	GTCACAAGGTGCATGGTGGA	20	1950	1969	652995	*UCA1*	Even
NR_015379	GGGCAGCTTTATAGGGCTTG	20	2022	2041	652995	*UCA1*	Even
NR_015379	CCAATCAGGCTTTGTGTGAG	20	2117	2136	652995	*UCA1*	Even
NR_015379	AGGAAAGGAAAACCACATGA	20	2244	2263	652995	*UCA1*	Even
NR_004430.2	CTCCCCTGCCAGGTAAGTAT	20	1	20	26871	*U1*	

All the antisense DNA probes are labeled with biotin at the 3' end.

Table S5. iRAP peptide sequences, Related to Figure 5

Sequence	Proteins	Start	End	*U1*	*UCA1-Odd1*	*UCA1-Even1*	*UCA1-Odd2*	*UCA1-Even2*
GGGGGQDNGLEGLGNDSR	sp|P08621|RU17_HUMAN	394	411	5	2			
ASMQQQQQLASAR	sp|Q9Y3Y2|CHTOP_HUMAN	39	51	4				
AVQGGGATPVVGAVQGPVPGMPPMTQAP	sp|P09012|SNRPA_HUMAN	124	152	4	1			
EEEIAALVIDNGSGMCK	sp|P63261|ACTG_HUMAN	2	18	3			1	
MMLGTEGGEGFVVK	sp|P31943|HNRH1_HUMAN	1	14	3				
NMGGPYGGGNYGPGGSGGSGGYGGR	sp|P22626|ROA2_HUMAN	326	350	3	1			
QEMQEVQSSR	sp|P22626|ROA2_HUMAN	191	200	3				
QQEVETELK	sp|P08621|RU17_HUMAN	79	87	3	2			
RGGADVNIR	sp|P08621|RU17_HUMAN	201	209	3	1			
RQQEVETELK	sp|P08621|RU17_HUMAN	78	87	3				
STVHEILCK	sp|P07355|ANXA2_HUMAN;sp|A	2	10	3	1		1	
ESTGAQVQVAGDMLPNSTER	sp|Q15365|PCBP1_HUMAN;sp|Q1	125	144	2				
SEMTPEELQK	sp|P62316|SMD2_HUMAN	9	18	2				
TDYNASVSVPDSSGPER	sp|P61978|HNRPK_HUMAN	70	86	2				
DSYVGDEAQSKR	sp|P60709|ACTB_HUMAN;sp|P63	51	62	2				
VEADRPGK	sp|P38159|RBMX_HUMAN;sp|Q9	2	9	2				
DSYESYGNSR	sp|P38159|RBMX_HUMAN;sp|Q9	283	292	2				
DGMDNQGGYGSVGR	sp|P31942|HNRH3_HUMAN	288	301	2				
NQGGYGGSSSSSSYGSGR	sp|P09651|ROA1_HUMAN	353	370	2				1
MWDPHNDPNAQGDAFK	sp|P08621|RU17_HUMAN	88	103	2				
VNYDTTESKLR	sp|P08621|RU17_HUMAN	110	120	2				
MIAGQVLDINLAAEPK	sp|P07910|HNRPC_HUMAN	74	89	2				
SLKLQASNVTNKNDPK	sp|Q9UKM9|RALY_HUMAN	2	17	1				
HRSCNTDDCPPGSQDFREVQCSEFDSIPFR	sp|Q9H324|ATS10_HUMAN	593	622	1				
MSATSVDTQR	sp|Q9BYJ9|YTHD1_HUMAN	1	10	1	1	1		
VADLTEQYNEQYGAVR	sp|Q9BWF3|RBM4_HUMAN	183	198	1				
EVYQQQQYGSGGR	sp|Q99729|ROAA_HUMAN	233	245	1				
EGSIEIDIPVPK	sp|Q96RQ3|MCCA_HUMAN	624	635	1				
IIEEAPAPGIK	sp|Q96RQ3|MCCA_HUMAN	285	295	1				
YLSSVSSQETQGGPLAPMTGTIEK	sp|Q96RQ3|MCCA_HUMAN	636	659	1	1			
TMFENVTR	sp|Q96QA5|GSDMA_HUMAN	2	9	1				1
AGGGPTLQCPPPSSPEK	sp|Q96N66|MBOA7_HUMAN	272	288	1				
KIQNDAGVR	sp|Q92945|FUBP2_HUMAN;sp|Q9	347	355	1				
DAFADAVQR	sp|Q92945|FUBP2_HUMAN	72	80	1				
IGGGIDVPVPR	sp|Q92945|FUBP2_HUMAN	321	331	1				
IGQQPQQPGAPPQQDYTK	sp|Q92945|FUBP2_HUMAN	629	646	1				
SDYSTGGPPPGPPPPAGGGGGAGGAGGGPP	sp|Q92945|FUBP2_HUMAN	2	40	1				
SVSLTGAPESVQK	sp|Q92945|FUBP2_HUMAN	191	203	1				
VQISPDSGGLPER	sp|Q92945|FUBP2_HUMAN	178	190	1				
APILIATDVASR	sp|Q92841|DDX17_HUMAN;sp|P1	469	480	1				
DMVGIAQTGSGK	sp|Q92841|DDX17_HUMAN	210	221	1				
SSQSSSQQFSGIGR	sp|Q92841|DDX17_HUMAN	671	684	1				
VLEEANQAINPK	sp|Q92841|DDX17_HUMAN	536	547	1				
EQMEKVEADLTR	sp|Q8N8E3|CE112_HUMAN	623	634	1				
QDNTPKR	sp|Q8N118|CP4X1_HUMAN	275	281	1				1
RLASPSEETWITCDNK	sp|Q86VB7|C163A_HUMAN	913	928	1				
DLQEQNKK	sp|Q5TB80|CE162_HUMAN	733	740	1	1	1	1	1
VAPDEHPILLTEAPLNPK	sp|Q562R1|ACTBL_HUMAN	97	114	1				
GGSYSQAASSDSAQGSDVSLTA	sp|Q31612|1B73_HUMAN	342	363	1				
VLVDQTTGLSR	sp|Q15717|ELAV1_HUMAN	137	147	1				
QKNKSGETVVLK	sp|Q15652|JHD2C_HUMAN	2249	2260	1				
INISEGNCPER	sp|Q15365|PCBP1_HUMAN;sp|Q1	47	57	1				
MQSNKTFNLEK	sp|Q15233|NONO_HUMAN	1	11	1				
SSSVGSSSSYPISPAVSR	sp|Q15149|PLEC_HUMAN	4384	4401	1				
AAAAVQGGR	sp|Q15005|SPCS2_HUMAN	2	10	1				
IFVGGLSPDTPEEK	sp|Q14103|HNRPD_HUMAN	184	197	1				
SSGGSYRDSYDSYATHNE	sp|Q14011|CIRBP_HUMAN	155	172	1				
AASAAAASAAAASAASGSPGPGEGSAGGE	sp|Q13263|TIF1B_HUMAN	2	32	1				
VLVNDAQK	sp|Q13263|TIF1B_HUMAN	312	319	1				
AATASAGAGGIDGKPR	sp|Q02978|M2OM_HUMAN	2	17	1				
GDATVSYEDPPTAK	sp|Q01844|EWS_HUMAN	411	424	1				
ATVQQLEGR	sp|Q01469|FABP5_HUMAN	2	10	1	1			
SSGPTSLFAVTVAPPGAR	sp|Q00839|HNRPU_HUMAN	187	204	1				
IQTQPGYANTLR	sp|Q00325|MPCP_HUMAN	190	201	1				
MIQVYFPK	sp|P82650|RT22_HUMAN	192	199	1				
AADPPAENSSAPEAEQGGAE	sp|P67809|YBOX1_HUMAN	305	324	1				
GAEAANVTGPGGVPVQGSK	sp|P67809|YBOX1_HUMAN	119	137	1				
GENLVSMTVEGPPPKDTGIAR	sp|P63162|RSMN_HUMAN;sp|P14	74	94	1				
TITLEVEPSDTIENVK	sp|P62987|RL40_HUMAN;sp|P629	12	27	1				
AAQGEPQVQFK	sp|P62826|RAN_HUMAN	2	12	1				
ECTIEATA	sp|P62633|CNBP_HUMAN	170	177	1				
SSNECFKCGR	sp|P62633|CNBP_HUMAN	2	11	1				
VAQLEQVYIR	sp|P62318|SMD3_HUMAN	55	64	1				
GDNITLLQSVSN	sp|P62304|RUXE_HUMAN	81	92	1				
ADIQTER	sp|P62280|RS11_HUMAN	2	8	1			1	
EITALAPSTMK	sp|P60709|ACTB_HUMAN;sp|P63	316	326	1				
AGFAGDDAPR	sp|P60709|ACTB_HUMAN;sp|P63	19	28	1	1		1	1

14

Peptide	Protein	Start	End						
DDDIAALVVDNGSGMCK	sp|P60709|ACTB_HUMAN	2	18	1					
HTGPNSPDTANDGFVR	sp|P55795|HNRH2_HUMAN;sp|P3	99	114	1					
MMLSTEGR	sp|P55795|HNRH2_HUMAN	1	8	1					
MLGPEGGEGFVVK	sp|P52597|HNRPF_HUMAN	2	14	1					
MGPAMGPALGAGIER	sp|P52272|HNRPM_HUMAN	592	606	1					
QGGGGGGGSVPGIER	sp|P52272|HNRPM_HUMAN	389	403	1					
SSGSPYGGGYGSGGGSGGYGSR	sp|P51991|ROA3_HUMAN	355	376	1					
ALVDGPCTQVR	sp|P50914|RL14_HUMAN	36	46	1					
ATTATMATSGSAR	sp|P38919|IF4A3_HUMAN	2	14	1		1			
DDGYSTKDSYSSRDYPSSR	sp|P38159|RBMX_HUMAN;sp|Q9	211	229	1					
DVYLSPR	sp|P38159|RBMX_HUMAN;sp|Q9	204	210	1					
YDDYSSSR	sp|P38159|RBMX_HUMAN;sp|Q9	310	317	1					
RGPPPPPR	sp|P38159|RBMX_HUMAN	94	101	1					
SDLYSSGR	sp|P38159|RBMX_HUMAN	332	339	1					
GEATVSFDDPPSAK	sp|P35637|FUS_HUMAN;sp|Q928	335	348	1					
GLPWSCSADEVQR	sp|P31943|HNRH1_HUMAN	17	29	1					
MLGTEGGEGFVVK	sp|P31943|HNRH1_HUMAN	2	14	1					
MLGTEGGEGFVVKVR	sp|P31943|HNRH1_HUMAN	2	16	1					
STGEAFVQFASK	sp|P31942|HNRH3_HUMAN	56	67	1					
DTSSSTVVSTQR	sp|P31483|TIA1_HUMAN	90	101	1					
FGQGGAGPVGGQGPR	sp|P23246|SFPQ_HUMAN	667	681	1					
MEKTLETVPLER	sp|P22626|ROA2_HUMAN	1	12	1					
TLETVPLER	sp|P22626|ROA2_HUMAN	4	12	1					
SISLYYTGEK	sp|P19338|NUCL_HUMAN	458	467	1					
AGEAPTENPAPPTQQSSAE	sp|P16989|YBOX3_HUMAN	354	372	1					
SEAGEATTTTTTTLPQAPTEAAAAAPQDPA	sp|P16989|YBOX3_HUMAN	2	33	1					
DNEETGFGSGTR	sp|P15144|AMPN_HUMAN	924	935	1					
AEAEAQAEELSFPR	sp|P11498|PYC_HUMAN	929	942	1					
ALAVSDLNR	sp|P11498|PYC_HUMAN	1062	1070	1					
SKSESPKEPEQLR	sp|P09651|ROA1_HUMAN	2	14	1					
DGGAWGTEQR	sp|P09382|LEG1_HUMAN	65	74	1					1
EVSSATNALR	sp|P09012|SNRPA_HUMAN	61	70	1					
IQYAKTDSDIIAK	sp|P09012|SNRPA_HUMAN	84	96	1					
KAVQGGGATPVVGAVQGPVPGMPPMTQA	sp|P09012|SNRPA_HUMAN	123	152	1		1	1		
TDSDIIAK	sp|P09012|SNRPA_HUMAN	89	96	1					
AETREERMER	sp|P08621|RU17_HUMAN	60	69	1					
DPIPYLPPLEK	sp|P08621|RU17_HUMAN	17	27	1					
GGADVNIR	sp|P08621|RU17_HUMAN	202	209	1					
GSERGRDEAR	sp|P08621|RU17_HUMAN	384	393	1					
IHMVYSK	sp|P08621|RU17_HUMAN	132	138	1					
KEELRGGGGDMAEPSEAGDAPPDDGPPGE	sp|P08621|RU17_HUMAN	306	346	1	1				
VLVDVER	sp|P08621|RU17_HUMAN	174	180	1	1				
AAVAGEDGR	sp|P07910|HNRPC_HUMAN;sp|P0	65	73	1					
ASNVTNKTDPR	sp|P07910|HNRPC_HUMAN	2	12	1					
VPPPPPIAR	sp|P07910|HNRPC_HUMAN	143	151	1					
AMGEQAVALAR	sp|P05165|PCCA_HUMAN	315	325	1					
MADALDNYVIR	sp|P05165|PCCA_HUMAN	466	476	1					
MADEAVCVGPAPTSK	sp|P05165|PCCA_HUMAN	105	119	1					
VVEEAPSIFLDAETR	sp|P05165|PCCA_HUMAN	299	313	1					
SGAQASSTPLSPTR	sp|P02545|LMNA_HUMAN	12	25	1					
MEDSASASLSSAAATGTSTSTPAAPTAR	sp|O76021|RL1D1_HUMAN	1	28	1					
TGYTLDVTTGQR	sp|O60506|HNRPQ_HUMAN;sp|O	131	142	1					
MEKENQKLEASR	sp|O60343|TBCD4_HUMAN	856	867	1					
PAASITSKPATLTTTSATSK	sp|O43670|ZN207_HUMAN	343	362	1					
NDNQETAAMKPENLKK	sp|A2A2Z9|AN18B_HUMAN	266	281	1					
QMEEELLFLK	tr|Q8WYG7|Q8WYG7_HUMAN	12	21						1
STILQQQFNR	sp|Q9Y4G6|TLN2_HUMAN	432	441		1	1			
QTDAQSASSPKK	sp|Q9Y3R0|GRIP1_HUMAN	754	765			1			
GVLQQGAGALGSSAQGVK	sp|Q9H8X9|ZDH11_HUMAN	297	314		1				
GGGEQETQELASK	sp|Q96QR8|PURB_HUMAN	25	37		1				
SSGQMAQKFSFSK	sp|Q96Q89|KI20B_HUMAN	105	117				1		
MKQKQEVMFQSR	sp|Q96LM1|CL037_HUMAN	1	12						1
DGAILCQPYITNGSLSLGVCGPQGR	sp|Q96BF3|TMIG2_HUMAN	62	86						1
STEPKMETMR	sp|Q8WTQ4|CP078_HUMAN	197	206				1		
SLQKEGFWPEAFSEVAEK	sp|Q8N9N8|EIF1A_HUMAN	95	112		1	1			
DQAEQWLR	sp|Q8N4X5|AF1L2_HUMAN	257	264		1	1			
FYEMYLLINK	sp|Q8IZJ1|UNC5B_HUMAN	577	586		1				
NSLSSIMKNKDK	sp|Q8IY51|TIGD4_HUMAN	51	62				1		
KNDQALQLTQMDKMHK	sp|Q86Z20|CC125_HUMAN	337	352				1		
GSGSGQSPSYGR	sp|Q86YZ3|HORN_HUMAN;CON	897	908						1
HGSSSGSSSR	sp|Q86YZ3|HORN_HUMAN;CON	2149	2158				1		1
QGSSAGSSSSYGQHGSGSR	sp|Q86YZ3|HORN_HUMAN;CON	507	525				1		
YGQQGSGSGQSPSR	sp|Q86YZ3|HORN_HUMAN;CON	649	662						1
FEVNAKFLGVDMER	sp|Q86VI3|IQGA3_HUMAN	1575	1588		1	1			
DVDAAYVSK	sp|Q7Z794|K2C1B_HUMAN;CON	274	282				1		1
VTVQTDDSNK	sp|Q6ZP68|ATPUN_HUMAN	105	114						1
SGTNNHVTVAIEN	sp|Q5W0Z9|ZDH20_HUMAN	353	365				1		1
QESTSKADLNCSKNK	sp|Q5W0B1|RN219_HUMAN	328	342				1		
IQSSQPMSLK	sp|Q5U4N7|GDF5O_HUMAN	2	11				1		
IEISSPCCPR	sp|Q5T749|KPRP_HUMAN	327	336				1	1	1
CQEEFWIR	sp|Q5FWF4|ZRAB3_HUMAN	940	947					1	1

Peptide	Protein	Start	End					
FSNSSSSNEFSK	sp|Q5D862|FILA2_HUMAN;CON	404	415					1
AGSLQLSSMSAGNSSLR	sp|Q53SF7|COBL1_HUMAN	380	396		1	1		
IQKEEEEILMANKR	sp|Q4VCS5|AMOT_HUMAN	727	740	1	1			1
DMLMQER	sp|Q3ZCV2|CA177_HUMAN	391	397		1	1		1
MEPIYPFARPQMNTR	sp|Q15468|STIL_HUMAN	1	15	1	1			
ERDAALK	sp|Q14980|NUMA1_HUMAN	598	604					1
NEWRMITAMNTIR	sp|Q14145|KEAP1_HUMAN	495	507	1				
KPEYDLEEDDQEVLK	sp|Q13416|ORC2_HUMAN	52	66	1				
MQLDNPSK	sp|Q13085|ACACA_HUMAN	818	825	1				
NVLLNNSEK	sp|Q08J23|NSUN2_HUMAN	569	577	1	1			
ENAGEDPGLAR	sp|P81605|DCD_HUMAN	43	53	1	1			1
DSYVGDEAQSK	sp|P60709|ACTB_HUMAN;sp|P63	51	61				1	1
MNALDLNMKTK	sp|P30519|HMOX2_HUMAN	206	216		1			
GGGGNFGPGPGSNFR	sp|P22626|ROA2_HUMAN	214	228	1	1			
NLKNSQMCQK	sp|P21439|MDR3_HUMAN	670	679				1	
NMLSQVNYRVPNMR	sp|P19174|PLCG1_HUMAN	179	192	1	1			
RQQLNEMLK	sp|P11532|DMD_HUMAN	2572	2580				1	
KNSYMNPEKK	sp|P08473|NEP_HUMAN	737	746		1			
AQGYSGLSVK	sp|P07996|TSP1_HUMAN;CON__	1055	1064				1	
GPDPSSPAFR	sp|P07996|TSP1_HUMAN;CON__	51	60				1	
GTSQNDPNWVVR	sp|P07996|TSP1_HUMAN;CON__	969	980				1	
SSPVVIDASTAIDAPSNLR	sp|P02751|FINC_HUMAN	1892	1910				1	1
TSLDEALQWR	sp|O15539|RGS5_HUMAN	53	62	1	1			
VAASIGNAQK	sp|O00151|PDLI1_HUMAN	247	256	1				

The numbers under each probe are the peptide hits obtained by mass spectrometry for iRAP protein samples.

Table S6. Antibody information used in this study, Related to Figure 4, 5, & 6

ANTIBODY	SOURCE	IDENTIFIER	NOTE
β-tubulin	Sigma Aldrich	Cat#T8328, RRID: AB_1844090	1:2,000
U1-70k	EMD Millipore	Cat#05-1588, RRID: AB_10805959	1:1,000
AMOT	Bethyl laboratories	Cat#A303-305A, RRID: AB_10951678	1:500
AXL	R&D Systems	Cat#AF-154, RRID: AB_354852	1:1,000
CYR61	Cell Signaling Technology	Cat#14479S, RRID: N/A	1:1,000
CTGF	Abcam	Cat# ab6992, RRID: AB_305688	1:1,000
YAP	Santa Cruz	Cat#sc-15407, RRID: AB_2273277	1:100-1,000, WB
YAP	Cell Signaling Technology	Cat#4912S, RRID: AB_2218911	IP
YAP (phosphoS127)	Abcam	Cat#ab76252, RRID: AB_1524578	1:1,000
Phospho-LATS1	Cell Signaling Technology	Cat#8654S, RRID: AB_10971635	1:100
LATS1	Cell Signaling Technology	Cat#3477T, RRID: AB_2133513	1:500
GFP	Santa Cruz	Cat#sc-9996, RRID: AB_627695	1:2,000
GAPDH	Fitzgerald Antibody	Cat#10R-G109A, RRID: AB_1285808	1:2,000
β-actin	Santa Cruz	Cat#sc-47778, RRID: AB_626632	1:2,000
Rabbit IgG	Thermo Fisher Scientific	Cat#10500C, RRID: AB_2532981	IP

Transparent Methods

Cell Culture. FTSEC33 and FTSEC246 cells were grown in DMEM/F12 media supplied with 10% FBS (HyClone, catalogue number: SH3007103) and L-glutamine. OSEC4 and OSEC11 were cultured in NOSE-CM media consisting of MCDB105: Medium 199 (1:1), 15% FBS, 10 ng/mL epidermal growth factor (Sigma Aldrich, catalogue number: E9644-2MG), 0.5 mg/mL hydrocortisone (Sigma Aldrich, catalogue number: H0888), 5 mg/mL insulin (Sigma, catalogue number: I1882-100MG), and 34 mg protein/mL bovine pituitary extract (Thermo Fisher Scientific, catalogue number: 13028014). CaOV3 cells were grown in RPMI1640 supplied with 10% FBS and L-glutamine. OVCA429 cells were cultured in EMEM supplied with 10% FBS, L-glutamine, sodium pyruvate (Lonza, catalogue number: 13-115E), and nonessential amino acids (Lonza, catalogue number: 13-114E). UWB1.289 cells were grown in mammary epithelial growth medium (MEGM): RPMI1640 (1:1) supplied with 3% FBS. HEK293T cells were cultured in DMEM supplied with 10% FBS.

H3K27ac ChIP-Seq and Super-enhancer Identification. H3K27ac ChIP-Seq and data analysis for primary ovarian cancer specimens were performed as described previously (Lawrenson et al., 2018). H3K27ac ChIP-Seq data for FTSEC33, FTSEC246, OSEC4, and OSEC11 are publicly available (Coetzee et al., 2015). The AQUAS pipeline (https://github.com/kundajelab/chipseq_pipeline) was used to processed ChIP-Seq data. Reads were aligned to the reference human genome (hg19), filtered by read quality and duplicate reads removed. MACS2 (https://pypi.python.org/pypi/MACS2) was used for peak calling. For the cell lines, two technical replicates were generated and the final peaks were obtained using a naive overlap approach, where the peaks are included if they overlap more than 50% between the two technical replicates. After alignment, homer (http://homer.ucsd.edu/homer/) was used to identify super-enhancers, using a super slope parameter of 2 and a minimum distance of ten thousand base pairs. For defining a set of high-grade serous ovarian cancer super-enhancers, we selected super-enhancers that were called in at least two high-grade serous ovarian cancer samples. For the FTSEC and OSEC sets of super-enhancers, super-enhancers were called individually in each technical replicate, then all the super-enhancers that overlapped both technical replicates within the same cell

line were selected to get the union set. To identify super-enhancer-associated lncRNAs, we directly overlapped the expressed lncRNAs with super-enhancers in high-grade serous EOC.

Survival and Super-enhancer-association Analysis. We used the superpc R package to perform the survival analysis using data from profiling of high-grade serous EOCs performed by TCGA (Cancer Genome Atlas Research, 2011). As training set 80% of the samples were randomly selected (377 samples) and the other 20% (77 samples) were used as the test set. Information about vital status was obtained from TCGA. We defined the threshold parameter as 1.4, n.components=3 and prediction.type="continuous". The significant genes were obtained in order of decreasing importance score. Super-enhancer domains in each cell line were identified using published procedures (Lovén et al., 2013; Whyte et al., 2013). To associate super-enhancers to lncRNAs we used the GenomicFeatures package (version 1.28.4) to manipulate the enhancer and lncRNAs genomic annotations. Gene coordinates were obtained using TxDb.Hsapiens.UCSC.hg19.knownGene (version 3.2.2) and org.Hs.eg.db (version 3.4.1) libraries.

RNA-Seq Data Generation and Analysis. Primary ovarian cancer specimens were homogenized and total RNA was extracted using TRIzol LS (Thermo Fisher Scientific, catalogue number: 10296028). Ribosomal RNA (rRNA) was depleted using RiboMinus Transcriptome Isolation Kit (Thermo Fischer Scientific, catalogue number: K155002). Poly (A)+ RNA was then isolated using Dynabeads Oligo (dT)$_{25}$ (Thermo Fischer Scientific, catalogue number: 61002). Twenty nanograms rRNA-poly (A)+ RNA was used to prepare each RNA-Seq library. External RNA Controls Consortium (ERCC) spike-ins (Thermo Fischer Scientific, catalogue number: 4456740) were added as control for normalization of the samples. Strand-specific RNA-Seq libraries were constructed using the NEBNext Ultra Directional RNA Library Prep Kit (NEB, catalogue number: E7420). The resulting library concentrations were quantified using the Nanodrop. Libraries were sequenced to generate paired-end 75 bp reads on NextSeq 500 platform (Illumina) in high output running mode. Sequencing was performed at the Molecular Genomics Core facility at the University of Southern California. RNA-Seq data were analyzed using Partek Flow and Partek Genomics Suite software after mapping reads to reference lncRNA gene mode (Gencode V16) with Tophat2.

Data Availability. H3K27ac ChIP-Seq data for normal precursor cells and primary tumors as well as RNA-Seq data for primary tumors have been deposited in the Gene Expression Omnibus database (GEO: GSE121103).

(+)-JQ1 treatment of the ovarian cancer cells. CaOV3 or UWB1.289 cells were treated with 10 nM (+)-JQ1 (Tocris, catalogue number: 4499) or an equal volume of DMSO (Sigma Aldrich, catalogue number: D2650) for 16 h before harvesting for RNA extraction.

Reverse transcription and real time quantitative PCR (RT-qPCR). RNA was extracted using TRIzol LS (Thermo Fisher Scientific, catalogue number: 10296028). M-MLV reverse transcriptase (Promega, catalogue number: M5301) and random hexamers (Promega, catalogue number: C1181) were used for reverse transcription. Gene expression was quantified by RT-qPCR using iQ SYBR Green supermix (Bio-Rad, catalogue number: 170-8886). The relative gene expression was calculated using the $2^{-\Delta\Delta Ct}$ method (Schmittgen and Livak, 2008). Two hundred and fifty nanograms cDNA was used for RT-qPCR analysis on CFX96 Touch Real-Time PCR Detection System (Bio-Rad) using the following primer pairs. *UCA1*-F: 5'CTTCTGCATAGGATCTGCAATCAG3', *UCA1*-R: TTTTGTCCCCATTTTCCATCATACG. *U1*-F: CCAGGGCGAGGCTTATCCATT, *U1*-R: GCAGTCCCCCACTACCACAAAT. *U6*-F: GCTTCGGCAGCACATATACTAAAAT, *U6*-R: CGCTTCACGAATTTGCGTGTCAT. *AXL*-F: GGTGGCTGTGAAGACGATGA, *AXL*-R: CTCAGATACTCCATGCCACT. *CYR61*-F: AAACCCGGATTTGTGAGGT, *CYR61*-R: GCTGCATTTCTTGCCCTTT. *OR10H1*-F: CCCAAAAGTCCCCAGTCTCT, *OR10H1*-R: CTCCTTGTTCCTGAGGCTGA. *GAPDH*-F: TGCCAAATATGATGACATCAAGAA, *GAPDH*-R: GGAGTGGGTGTCGCTGTTG, *18S*-F: CAGCCACCCGAGATTGAGCA, *18S*-R: TAGTAGCGACGGGCGTGTG, *β-actin*-F: TCACCCACACTGTGCCCATCTACGA, *β-actin*-R: CAGCGGAACCGCTCATTGCCAATGG.

CRISPR/Cas9 KO of *UCA1*. Guide RNAs (gRNAs) were designed using the CRISPR design tool (http://crispr.mit.edu/). Two gRNAs were cloned into PX458 (Addgene plasmid number 48138) - *UCA1* promoter: GGTTTCCTTTTAGATGACGG, *UCA1* intron: GGCTAGAATATTTGCAGGCG, following the methods of the Zhang laboratory (Ran et al., 2013). Target cells were co-transfected with the two gRNAs

expressing plasmids or the vector backbone only as a control, using the BioT transfection reagent (Bioland Scientific, catalog number: B01-01). Positive cells were isolated using an Aria II flow cytometer (BD Biosciences) to sort single cells into 96 well plates. For validation of the deletion, PCR was performed using Sequal Prep™ Long PCR Kit with the following primers - Forward: GACACTGCATTGTGTGCGTT, Reverse: TCCCTGTTGCTAAGCCGATG.

Mouse xenografts. All *in vivo* work was performed with the approval of the USC Institutional Animal Care and Use Committee. Ten million cells were injected with 25% Matrigel subcutaneously into female nu/nu mice (aged 6-8 weeks). Tumor growth was measured by digital caliper measurement and animals euthanized when tumor diameter reached >1.5 cm, or after 8 weeks.

RPPA. Cells were plated into 6 well plates overnight. Cells were washed with PBS and lysed for 20 minutes in buffer containing 1% Triton X-100, 50 mM HEPES, pH 7.4, 150 mM NaCl, 1.5 mM $MgCl_2$, 1 mM EGTA, 100 mM NaF, 10 mM Na pyrophosphate, 1 mM Na_3VO_4, 10% glycerol, plus PhosSTOP Protease Inhibitor Cocktail (Roche, catalog number: 4906837001) and Protease Inhibitor Cocktail (Roche, catalog number: 11873580001). Insoluble proteins were removed by centrifugation and normalized proteins denatured by boiling in 4× SDS sample buffer (40% Glycerol, 8% SDS, 0.25 M Tris-HCl, pH 6.8 plus 10% 2-mercaptoethanol).

iRAP. Two sets of UCA1 antisense DNA probes with 3' biotin labels were ordered from siTOOLs Biotech GmbH. A U1 antisense probe (Chu et al., 2015) was included as a positive control. OVCA429 were cultured on 150 mm tissue culture plates and used at 90% confluency 96 h after seeding. Cells were washed with 10 mL ice-cold PBS and crosslinked in the presence of 10 mL ice-cold PBS using a Stratalinker (UV Stratalinker 1800, Stratagene) at 254 nm wavelength with 0.8 J/cm2. Cells were collected and centrifuged at 1,000 g for 5 min at 4 °C. The supernatant was removed and cells used directly for iRAP or snap frozen in liquid nitrogen and stored at -80 °C until use. Cells were lysed in Lysis Buffer (10× the mass of pellet, 10 mM Tris-HCl, pH7.0, 50 mM EDTA, 1% SDS) containing freshly added PhosSTOP Protease Inhibitor Cocktail (Roche, catalog number: 4906837001) and Protease Inhibitor Cocktail (Roche, catalog number: 11873580001), PMSF (Sigma Aldrich, catalog number: 93482) and Superase-in (Ambion, catalog number: AM2696). Crosslinked cells were lysed

using a Covaris E220 evolution Focused-Ultrasonicator at 4 °C, 20% output, 200 burst cycles, for 15 min for each 20 million cells in 1 mL lysate buffer. Sonicated samples were centrifuged at 16,000 g for 10 min at 4 °C. Cell lysates representing 400 million cells were combined with 2 nM U1 or UCA1-odd/even probe sets in two volumes of hybridization buffer (750 mM NaCl, 1% SDS, 50 mM Tris-HCl pH 7.0, 1 mM EDTA, 15% formamide, with fresh PMSF, phosphatase inhibitor, proteinase inhibitor cocktail, and Superase-in). Hybridization was performed at 37 °C with rotation overnight. RNA-protein complexes were precipitated by adding 2 mL Streptavidin Dynabeads M-270 (Thermo Fisher Scientific, catalog number: 65036) for 30 min at 37 °C. Dynabeads were washed with 2×NaCl and sodium citrate (SSC), 0.5% SDS, and fresh PMSF for 5×5 min.

RIP. Twelve microliter Dynabeads Protein A (Thermo Fisher Scientific, catalog number: 10001D) were washed with 200 µL HBS (150 mM NaCl, 10 mM HEPES, pH7.5 by KOH and incubated with 2 µg AMOT antibody, 2 µg YAP antibody or 2 µg rabbit IgG isotype control in the presence of 80 µL HBS buffer at room temperature for 1 h. Eight million CaOV3, OVCA429, or UWB1.289 cells were lysed with 800 µL cell lysis buffer (10 mM HEPES, pH7.5 by KOH, 150 mM NaCl, 0.1% NP-40, 5 mM EGTA, supplemented with 1× protease inhibitor cocktail and Superase-in) at 4°C for 1 h. Cell debris and insoluble proteins were removed by centrifugation at 4°C, 12,000 g for 10 min, and the supernatants were incubated with antibody-conjugated Dynabeads at 4°C for 1 h. The Dynabeads were then washed 3 times with wash buffer (150 mM NaCl, 10 mM HEPES, pH7.5 by KOH, 0.1% NP-40). Half of the sample was eluted with 12 µL 1×Laemmli sample buffer (Bio-Rad, catalog number: 1610747) and used for Western blotting, TRIzol LS was added to the other half before proceeding with RNA extraction (Thermo Fisher Scientific, catalog number: 10296028).

Plasmids. Lenti GFP-AMOT p80 and lenti GFP-AMOT p130 were gifts from Dr. Kun-Liang Guan (Addgene plasmid numbers 32830 & 32828). To generate a *UCA1* overexpression plasmid, the full cDNA sequence for *UCA1* was purchased from Genewiz and cloned into the LeGO-iT vector. LeGO-iT was a gift from Dr. Boris Fehse (Addgene plasmid number 27361). Lentiviral particles were produced from co-transfecting HEK293T cells with LeGO-iT+*UCA1,* Lenti GFP-AMOT p80, or Lenti GFP-AMOT p130 together with lentiviral

packaging plasmids pMD2.G and psPAX2 (Gifts from Dr. Didier Trono, Addgene plasmid numbers 12259 & 12260). LeGO-iT has an IRES-tdTomato marker that was used for flow cytometric selection on Aria II cell sorter (BD Biosciences) after transduction.

Transfection. Pooled siRNAs targeting human *UCA1* (Dharmacon, catalog number: R-188002-00-0005), AMOT (Dharmacon, catalog number: L-015417-01-0005), YAP (Dharmacon, catalog number: L-012200-00-0005) or non-targeting scramble controls (Dharmacon, catalog number: D-001810-01-20) were transfected into CaOV3, UWB1.289, or OVCA429 cells using Lipofectamine RNAiMAX transfection reagent (Thermo Fisher Scientific, catalog number: 13778075), DharmaFECT 3 (Dharmacon, catalog number: T-2003-03), or DharmaFECT 1 transfection reagent (Dharmacon, catalog number :T-2001-03), respectively.

Cellular fractionation. Cells were fractionated as previously described (Bahn et al., 2015) with some modifications. Six million OVCA429 cells were treated with the plasma membrane lysis buffer (10 mM Tris-HCl, pH 7.5, 0.15% Nonidet P-40, 150 mM NaCl) on ice for 5 min after homogenization by flicking. For CaOV3 and UWB1.289 cells, six million cells were lysed for 4 min with lysis buffer and for OSEC4C2 cells, eight million cells were treated with lysis buffer for 2 min. Centrifuge at 15,000 g for 10 min at 4°C after loading the lysate onto 24% sucrose cushion (24% RNase-free sucrose in plasma membrane lysis buffer) using large orifice tips. The supernatant (cytoplasmic fraction) was retained after centrifugation, and the pellet (nuclear fraction) was washed with 1×PBS/1 mM EDTA and resuspended in 200 μL of 1×PBS/1 mM EDTA.

Western Blotting. Protein samples were run on 4-20% gradient precast protein gel (Bio-Rad, catalogue number: 456-1096) and transferred onto PVDF membrane (Bio-Rad, catalogue number: 1704157). After 1 h blocking, membranes were incubated with corresponding antibody at 4°C overnight. Membranes were washed three times with Tris-buffered saline containing 0.5% Tween 20 (TBST) before incubating with HRP-conjugated secondary antibody or Clean-Blot IP detection reagent (Thermo Fisher Scientific, catalogue number: 21230) for IP samples at room temperature for 2 h. Then the membranes were incubated briefly with ECL Western Blotting substrate (Thermo Fisher Scientific, catalogue number: 32106) after three times wash with

TBST. The membranes were exposed to HyBlot Autoradiography Film (Denville Scientific, catalogue number: E3018). Antibody information is listed in Supplementary Table 6.

Supplementary References

Bahn, J.H., Ahn, J., Lin, X., Zhang, Q., Lee, J.H., Civelek, M., Xiao, X., 2015. Genomic analysis of ADAR1 binding and its involvement in multiple RNA processing pathways. Nat Commun 6, 6355. https://doi.org/10.1038/ncomms7355

Cancer Genome Atlas Research, N., 2011. Integrated genomic analyses of ovarian carcinoma. Nature 474, 609–15. https://doi.org/10.1038/nature10166

Chu, C., Zhang, Q.C., da Rocha, S.T., Flynn, R.A., Bharadwaj, M., Calabrese, J.M., Magnuson, T., Heard, E., Chang, H.Y., 2015. Systematic discovery of Xist RNA binding proteins. Cell 161, 404–16. https://doi.org/10.1016/j.cell.2015.03.025

Coetzee, S.G., Shen, H.C., Hazelett, D.J., Lawrenson, K., Kuchenbaecker, K., Tyrer, J., Rhie, S.K., Levanon, K., Karst, A., Drapkin, R., Ramus, S.J., Ovarian Cancer Association Consortium, T.C. of I. of M. of B., Couch, F.J., Offit, K., Chenevix-Trench, G., Monteiro, A.N., Antoniou, A., Freedman, M., Coetzee, G.A., Pharoah, P.D., Noushmehr, H., Gayther, S.A., Ovarian Cancer Association Consortium The Consortium of Investigators of Modifiers of, B., 2015. Cell-type-specific enrichment of risk-associated regulatory elements at ovarian cancer susceptibility loci. Hum Mol Genet 24, 3595–607. https://doi.org/10.1093/hmg/ddv101

Lawrenson, K., Fonseca, M.A.S., Segato, F., Lee, J.M., Corona, R.I., Seo, J.-H., Coetzee, S., Lin, Y.G., Pejovic, T., Mhawech-Fauceglia, P., Drapkin, R., Karlan, B.Y., Hazelett, D.J., Freedman, M.L., Gayther, S.A., Noushmehr, H., 2018. Integrated Molecular Profiling Studies to Characterize the Cellular Origins of High-Grade Serous Ovarian Cancer. bioRxiv 330597. https://doi.org/10.1101/330597

Lovén, J., Hoke, H.A., Lin, C.Y., Lau, A., Orlando, D.A., Vakoc, C.R., Bradner, J.E., Lee, T.I., Young, R.A., 2013. Selective inhibition of tumor oncogenes by disruption of super-enhancers. Cell 153, 320–34. https://doi.org/10.1016/j.cell.2013.03.036

Ran, F.A., Hsu, P.D., Wright, J., Agarwala, V., Scott, D.A., Zhang, F., 2013. Genome engineering using the CRISPR-Cas9 system. Nat Protoc 8, 2281–308. https://doi.org/10.1038/nprot.2013.143

Schmittgen, T.D., Livak, K.J., 2008. Analyzing real-time PCR data by the comparative C(T) method. Nat Protoc 3, 1101–1108.

Whyte, W.A., Orlando, D.A., Hnisz, D., Abraham, B.J., Lin, C.Y., Kagey, M.H., Rahl, P.B., Lee, T.I., Young, R.A., 2013. Master transcription factors and mediator establish super-enhancers at key cell identity genes. Cell 153, 307–19. https://doi.org/10.1016/j.cell.2013.03.035